Analysis and optimization of acoustic wave micro-resonators integrating piezoelectric zinc oxide layers

Oussama Mortada, Abedel Halim Zahr, Jean-Christophe Orlianges, Aurelian Crunteanu, Matthieu Chatras, Pierre Blondy

Analysis and optimization of acoustic wave micro-resonators integrating piezoelectric zinc oxide layers

O. Mortada[1], A. H. Zahr[1], J-C. Orlianges[1], A. Crunteanu[1], M. Chatras[1] and P. Blondy[1]

[1] *XLIM UMR 7252, University of Limoges/ CNRS, 123 avenue Albert THOMAS, 87060 Limoges Cedex, FRANCE*

This paper reports on the design, simulation, fabrication and test results of ZnO-based contour-mode micro-resonators integrating piezoelectric zinc oxide (ZnO) layers. The inter-digitated (IDTs) type micro-resonators are fabricated on ZnO films and suspended top of 2µm thick silicon membranes using silicon-on insulator (SOI) technology. We analyze several possibilities of increasing the quality factor (*Q*) and the electromechanical coupling coefficient (k_t^2) of the devices by varying the numbers and lengths of the IDTs electrodes and using different thicknesses of the ZnO layer. We designed and fabricated IDTs of different finger numbers (*n=25, 40, 50 and 80*) and lengths (*L=100/ 130/ 170/ 200 µm*) for three different thicknesses of ZnO films (200, 600 and 800 nm). The measured *Q* factor confirms that reducing the length and the number of IDTs fingers enables to reach better electrical performances at resonant frequencies around 700 MHz. The extracted results for an optimized micro-resonator device having a IDTs length of 100 µm and 40 finger electrodes, show a *Q* of 1180 and a k_t^2 of 7.4%. We demonstrate also that the reduction of the ZnO thickness from 800 nm to 200 nm increases the quality factor from 430 to 1600 respectively, around 700 MHz. Experimental data are in very good agreement with theoretical simulations of the fabricated devices

I. INTRODUCTION

Acoustic filters are among the most compact devices that can be used for RF communication systems [1-3], and recent improvements of composite MEMS resonators enable to achieve very high quality factors *Q*, allowing for low-imprint devices and operating frequencies as high as 8 GHz [4][5]. A lot of research efforts were focused on bulk acoustic wave (BAWs) [6-8] devices which offered many potentialities for smart RF components or systems, especially as an alternative to surface acoustic waves (SAWs) filters [9][10].

Here we present a novel piezo-acoustic ZnO-based contour-mode device fabricated on suspended silicon membrane. The general structure of this type of resonator consists of metallic interdigitated (IDTs) electrodes acoustically coupled within a piezoelectric zinc oxide (ZnO) film suspended on monocrystalline (100) silicon membranes. The design optimization of such devices allows reaching high quality factor *Q* and high electromechanical coupling coefficient k_t^2 [11]. These two parameters are important factors for the integration of such piezoelectric micro-resonators for filter applications since they are key elements to achieve a high figure of merit which is directly associated with the quality factor and the electromechanical coupling coefficient ($FoM = k_t^2.Q$) [12].

This manuscript was accepted by J. Appl. Phys. Click here to see the version of record.

In this paper, a detailed study has been achieved on micro-resonators topology, in order to identify the optimum geometrical parameters (especially the length, the number of IDTs electrodes and the thickness of ZnO layer) affecting the micro-resonators performances. In order to study the effect of these parameters and experimentally checking their influence, we have designed, fabricated, and tested micro-resonators devices operating around 700 MHz. This frequency corresponds to the first excited acoustic mode displayed by a device incorporating a 500 nm thick ZnO layer and using IDTs with w_{pitch} = 4-µm electrode pitch (see Figure 1).

We investigated different IDTs lengths, (*L=12λ, 17λ, 21λ* and *25λ* corresponding to 100/130/170/200 µm), different numbers of IDTs electrodes (*n= 80/ 50/ 40/ 25)* on ZnO layers with thicknesses between 200 and 800 nm. We studied the influence of all these parameters on the extracted quality factor *Q* and the electromechanical coupling coefficient k_t^2 while comparing the measured responses of the micro-resonators to the simulated results obtained using the MBVD electrical model (Modified Butterworth Van Dyke).

The paper is organized as follows. In part II we present the design and the fabrication process followed by modeling techniques for this type of micro-resonators in part III. In part IV, the performance of these devices are experimentally investigated and compared to the theoretical analysis (electrical model) and to finite-element –modeling (FEM). We report and discuss (in parts V and VI) three key device performance parameters: power handling, nonlinear electrical characterization and temperature coefficient of frequency (TCF). Part VII concludes the paper by summarizing the contributions of our study and setting future perspectives for device implementation

II. ZINC OXIDE MICRO-RESONATORS: DESIGN AND FABRICATION

Figure 1 shows a cross-section of the proposed ZnO-based contour-mode micro-resonator. It is made with metal IDTs electrodes acoustically coupled to a suspended composite ZnO/Si structure. When a RF signal is applied across the IDTs, the piezoelectric layer moves perpendicularly to the substrate plane, leading to successive displacements and charge generation by acoustic pressure from the input to the output electrodes. In practice, the zinc oxide piezoelectric film is sandwiched between patterned gold top electrodes and a molybdenum (Mo) floating bottom electrode. By looking at Figure 1, two types of acoustic waves can be detected in these micro-resonators: some waves are propagating in the ZnO film; others are propagating in the silicon membrane. First ones are propagating in all the thickness of the ZnO layer, but the second ones are guided elastic waves, referred as two-dimensional Lamb waves or plate modes. They are highly dispersive, and have very high propagation speeds. It is clear that the excitation field induced by the combined electrode system makes it possible to optimize the selective electric transduction of these guided modes.

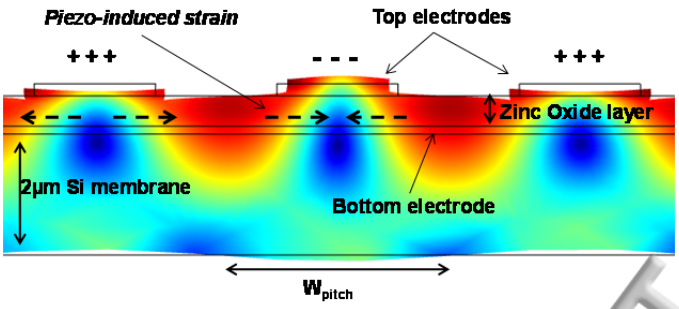

FIG. 1. Finite element method (FEM) simulation showing the membrane displacement during propagation of an acoustic wave in ZnO and Si membrane layers. The figure shows only few of the IDTs finger electrodes as representatives of the overall device behavior.

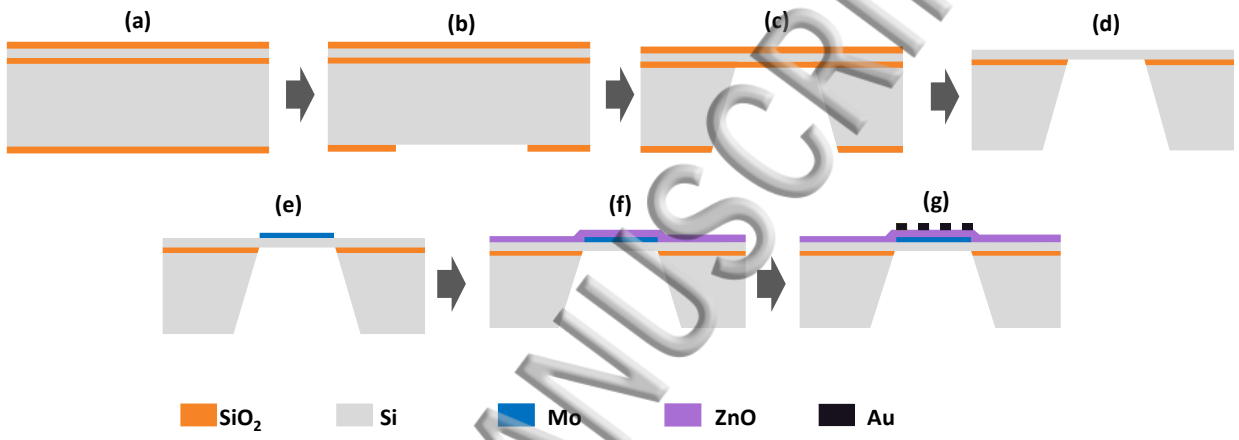

FIG. 2. Flow chart of the fabrication process: (a) used SOI wafers; (b),(c) backside etching to suspend the silicon membrane; (d) oxide layers (on the backside layer, below and above the silicon membrane) are removed by BOE (buffered oxide etch, HF based) solution; (e) sputtering and patterning of the Mo floating electrode; (f) deposition of ZnO thin film; (g) patterning of IDTs top electrode

For a given composite ZnO/Si resonator thickness, the mechanical resonance of such structure can be written [13]:

$$f_r = \frac{1}{2.w_p}\sqrt{\frac{E_{\text{eq}}}{\varphi_{\text{eq}}}} \quad (1)$$

where w_p is the electrode pitch, E_{eq} and φ_{eq} are the equivalent modulus of elasticity and mass density of the composite ZnO/Si layers.

The proposed micro-resonators are fabricated following the procedure shown in Figure 2. The three-mask fabrication process is conducted on low resistivity (30 Ω.cm) 2 µm thick SOI wafers. A 1 µm thick thermal oxide layer is grown on both sides of the SOI wafer, to serve as hard mask for further wafer bulk micromachining [14], but also for electrical isolation.

SOI wafers were used because of the high intrinsic Si material acoustic quality, near-zero built-in stress and predictable mechanical properties of the top single-crystal silicon layer, which is used as the suspended membrane [15]. The first processing step is back-side etching. A photolithography is carried to expose wafer back-side areas and SiO_2 is etched (Figure 2 (b)) using buffered hydrofluoric acid (BHF), followed by 450 µm deep silicon etching (Figure 2 (c)) using TMAH (Tetra Methylamine

Hydroxide) at 85°C. Etching is completed when the 2-µm thick Si membranes are released and suspended on the SOI substrate. Next, a 280 nm thick molybdenum (Mo) layer is DC sputtered on the wafer at 300°C (Figure 2 (d)). The bottom Mo electrode is then patterned, followed by the deposition of ZnO film layer by Pulsed Laser Deposition (Figure 2 (e)). The ZnO thin film show a pure (002) texture and the full width half maximum (FWHM) of the (002) diffraction peak is equal to 0.07°. More information and detailed description about the quality of deposited ZnO layer can be found in our previous work [11]. Lastly, inter-digital fingers (200 nm thick of Au) are deposited using the lift-off procedure on the ZnO surface (Figure 2 (f)). A close-up scanning electron microscope (SEM) images of the fabricated micro-resonators with different IDTs lengths and numbers can be seen in Figure 3.

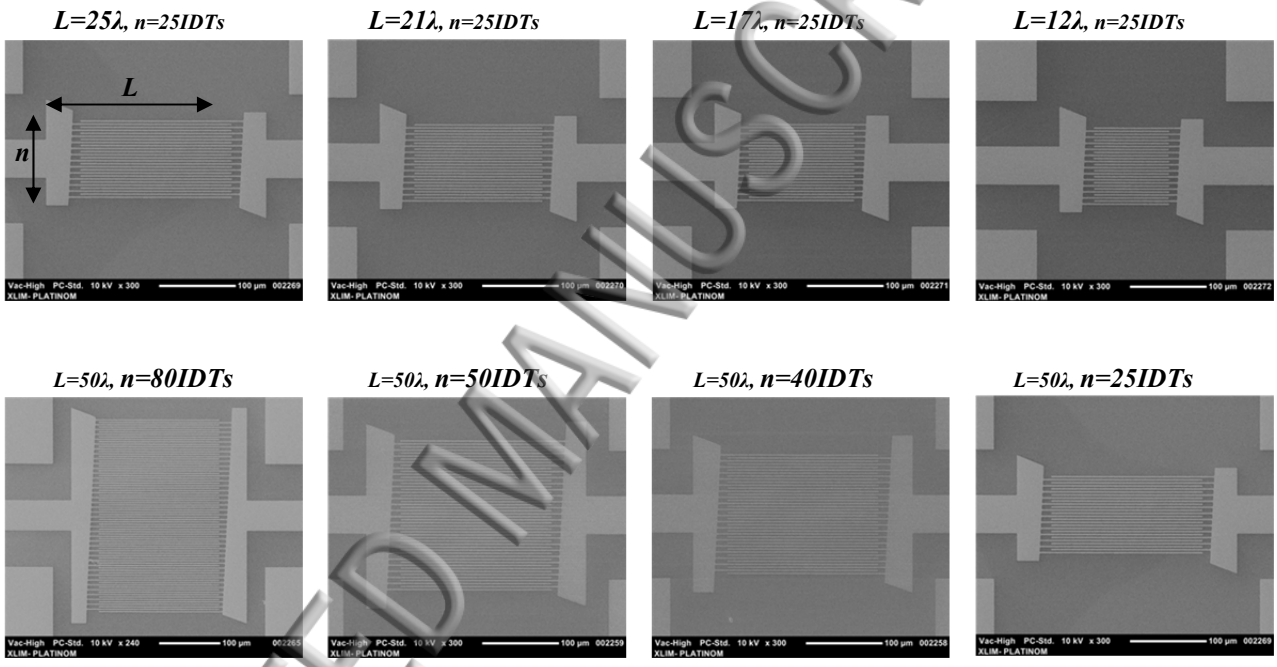

FIG. 3. SEM picture of the fabricated devices: eight micro-resonators having different lengths *L* of IDTs electrodes and different numbers *n* of IDTs electrodes.

III. MODELING AND SIMULATION

The measured responses of the fabricated devices were fitted to the Modified Butterworth van Dyke (MBVD) model shown in Figure 4, which expresses the electrical behavior of these piezoelectric micro-resonators and then equivalent electrical parameters were extracted.

This manuscript was accepted by J. Appl. Phys. Click here to see the version of record.

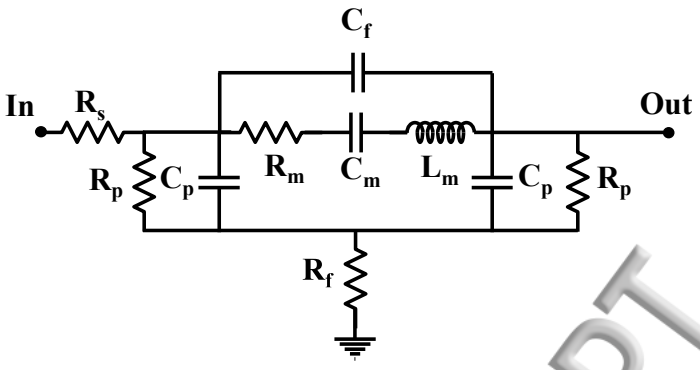

FIG. 4. The equivalent MBVD model considering all losses present in the structure.

The motional resistance R_m comes from the mechanical damping transformed to the electrical domain; C_m and L_m are motional capacitance and impedance respectively and used to represent, with R_m, the mechanical motion of the device. The capacitor C_f is added to account for the feedthrough between IDTs electrodes; it is a function of finger pitch (w_p), length (L) and spacing (w_s). C_p and R_p are respectively shunt capacitance and shunt resistance. C_p is determined by the static capacitance of the electrode areas and R_p represents loss from the leakage current and dielectric loss from the piezoelectric material. R_f expresses losses induced by the silicon membrane, this membrane is very low resistivity (30 Ω.cm). Lastly, R_s come from transmission line losses.

The quality factor Q was computed using the following equation [16]:

$$Q = \frac{1}{R_m}\sqrt{\frac{L_m}{C_m}} \tag{2}$$

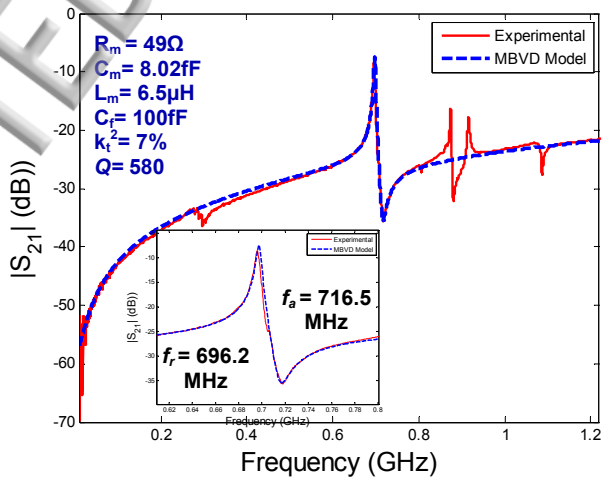

FIG. 5. Comparison between the measured S_{21} parameters and the corresponding MBVD model with parameters extraction for fabricated micro-resonators (n=25 & L=21λ)

This manuscript was accepted by J. Appl. Phys. Click here to see the version of record.

Figure 5 shows an example of comparison between the measured S_{21} parameters of a fabricated micro-resonator and the corresponding MBVD model. We can notice very good agreements. This transmission response shows two important frequencies: the resonant frequency f_r where the device behaves like a short circuit and the anti-resonance frequency f_a where it behaves like an open circuit. Outside these ranges of resonances, the micro-resonator behaves like a capacitance.

Following the FEM simulations it was deduced that the resonance appearing at 1.2 GHz belong to a silicon membrane bulk resonant mode while the modes between 0.8 and 1 GHz are spurious flexural modes coming from reflexions into the input/ output electrodes. These modes can be easily suppressed by modifying the micro-resonator geometry.

IV. DEVICE MEASUREMENTS

The fabricated prototypes have been tested using a ROHDE & SCHWARZ-ZVA24 Vector Network Analyzer and a Cascade probe station using GSG probes. Tested devices were directly probed and connected to the measurement instrumentation without the use of any external electronic interface. A short load open through (SLOT) calibration was performed.

A. *Q* Evolution for different lengths and numbers of IDTs

A theoretical study of the scattering [S] parameters was performed using the equivalent electrical model MBVD to extract the values of the electrical model components describing the micro- resonators. These values enables to calculate the quality factor Q, which will facilitate the interpretation of this analysis.

Figure 6 reports the average quality factor Q recorded from a collection of 12 combinations of n and L. Q is compared among the same IDTs lengths of micro-resonators having different number of IDTs. From the data represented on Figure 6 a clear trend relating the measured Q vs electrode number and length of IDTs is observed.

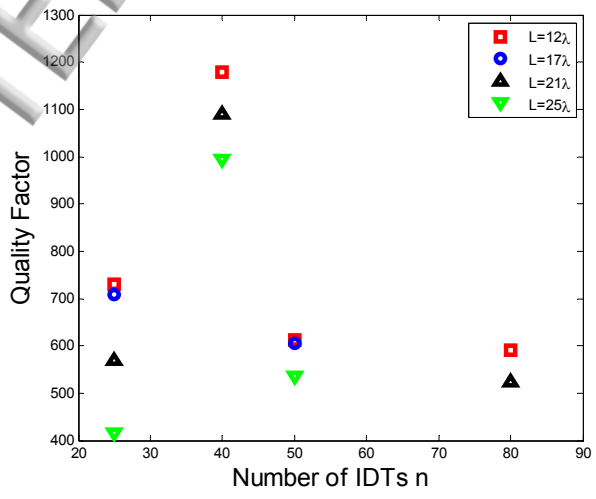

FIG. 6. Average variation of Q for 12 combinations of micro-resonators with four different IDTs number and four different IDTs lengths.

First, by comparing micro-resonators having the same IDTs number in Figure 6 (n = 25 IDTs for example), we can notice that decreasing IDTs length increases the quality factor, from 413 (for the 25λ IDTs length) to 730 (for the 12λ IDTs length).

Second, for a fixed IDTs length $L=12\lambda$, the quality factor increases from 730 (for n = 25 IDTs) up to 1180 (for $n=40$ IDTs) then down to 612 and to 590 for $n=50$ and $n=80$ respectively. We can notice a high peak quality factor when $n=40$ IDTs. This behavior is repeated for the other three lengths $L = 17\lambda$, 21λ and 25λ (Figure 6). The presented experimental results show that Q improves drastically when $n=40$ and the length $L=12\lambda$.

Looking at [S] parameters of the measured circuit presented in Figure 7, we noted the presence of spurious modes in close proximity of the main mechanical resonance of certain micro-resonators: micro-resonators having a large number of IDTs electrodes have a plurality of resonance modes which are mixed together at the main mechanical resonance so that the resonance peak becomes less selective and less "clean" which corresponds to a low Q.

2D FEM analysis was performed using COMSOL software in order to evaluate the experimental performances of these micro-resonators. Figure 7 shows a comparison between these simulations and measured micro-resonators. It shows how spurious modes appear and multiple when the number of IDTs is increasing. It is due to the reflected acoustic waves in the system, especially when the suspended Si membrane is large and the resonator includes a high number of IDTs (Figure 8).

By reducing the number of IDTs electrodes, resonance peaks are very selective because spurious modes are strongly attenuated especially for IDTs having $n=40$ which corresponds to the highest Q, and disappear completely when $n=25$ IDTs. On the other hand, when $n=25$, the equivalent motional impedance R_m increases dramatically and this is why the quality factor go down again.

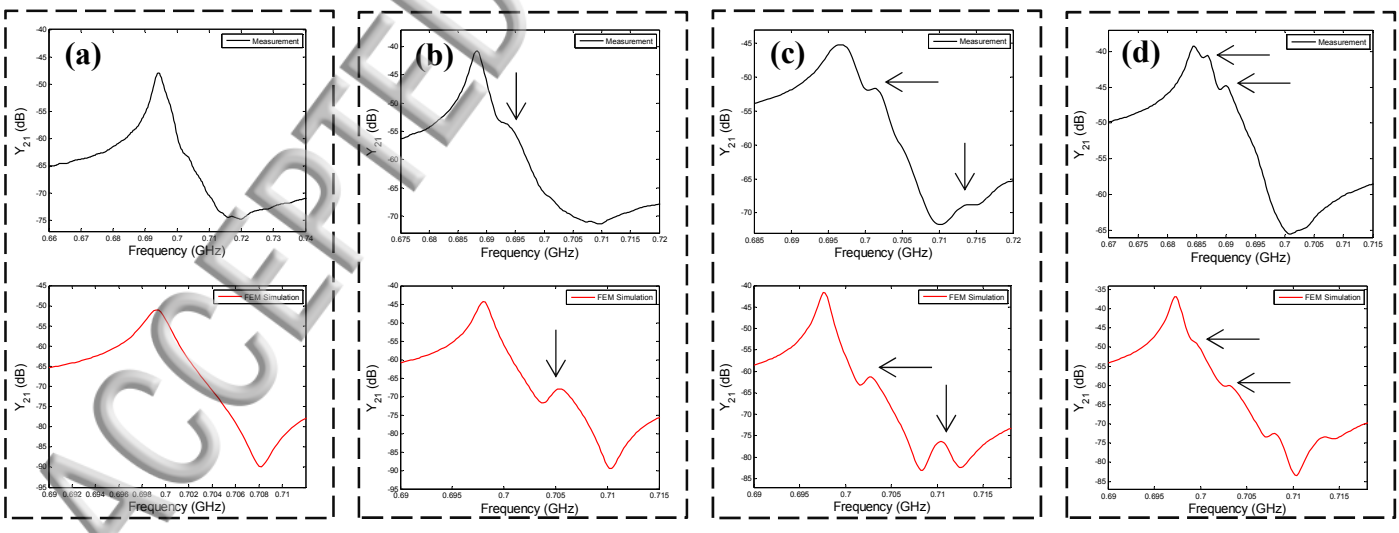

FIG. 7. Plot of measured and FEM simulated admittance response of four different micro-resonators: (a) with 25IDTs, (b) with 40IDTs, (c) with 50IDTs, (d) with 80IDTs. Spurious modes appear when the number of IDTs is increasing.

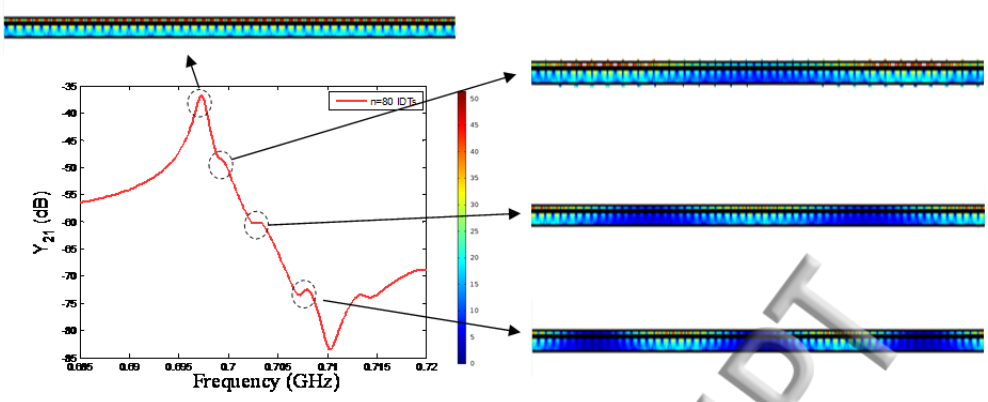

FIG. 8. Plot of simulated Y_{21} admittance response of a micro-resonator having 80 IDTs electrodes. Spurious modes appear due to the reflected acoustic waves in the system. The shape of acoustic waves propagating in the device for spurious modes is indicated by the arrows

B. Evolution of k_t^2 for different lengths and numbers of IDTs

The electromechanical coupling coefficient k_t^2 expresses the degree of energy interaction between the mechanical and electrical domains. According to (3), it depends on resonance and anti-resonance values:

$$k_t{}^2 = \frac{\pi^2}{4}\frac{f_a - f_r}{f_a} \tag{3}$$

k_t^2 measurement results and their evolution with the length and number of IDTs electrodes are shown in Figure 9. For a given length, the k_t^2 values decreased with increasing the number of IDTs electrodes. Thus, for a length $L=12\lambda$, the k_t^2 takes its largest value of 8.84% when the number of IDTs n is equal to 25 and this value decreases to 5.67% when n increases to 80. The same evolution is observed with $L= 21\lambda$, where k_t^2= 7% in the case of 25-n IDTs electrodes and decreases to 4.3% for 80-n IDTs electrodes.

This behavior does not only depend on the number of IDTs electrodes but also on their length. From the data represented on figure 8, we can also see that the k_t^2 varies also with the variation of IDTs electrode length: smaller lengths result in a greater coupling coefficient. For example, for 40-n IDTs, the k_t^2 decreases from 7.4% when $L=12\lambda$ to 5.34% when $L=25\lambda$.

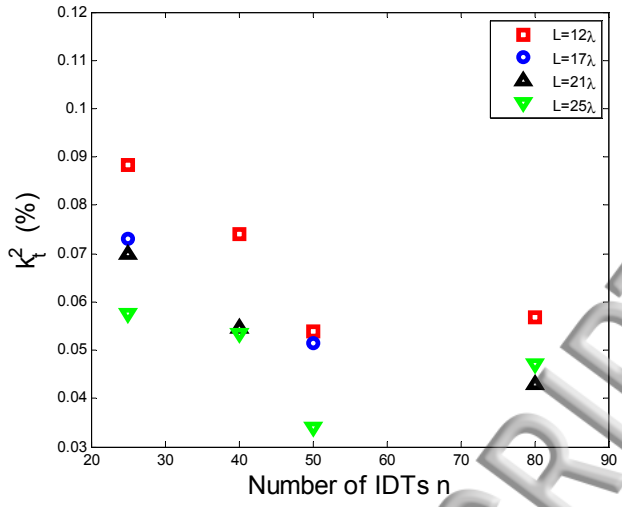

FIG. 9. Variation of k_t^2 from a sample of three equivalent circuits at 700MHz with four different IDTs electrodes number and four different IDTs lengths.

The figure of merit (FOM) can be calculated and is presented in Figure 10.

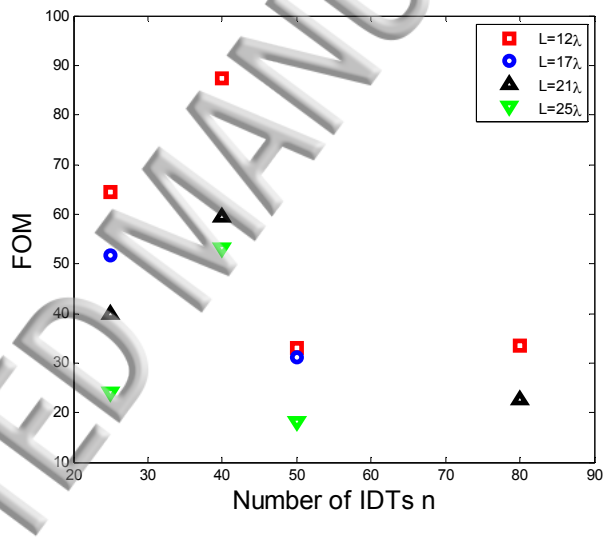

FIG. 10. Variation of *FOM* of contour-mode micro-resonators with four different IDTs electrodes number and four different IDTs lengths.

The optimization of n and L enabled a record-high electromechanical coupling k_t^2 of 7.4% with a high quality factor Q equal to 1180. This have been achieved by mechanically coupling 40-n IDTs of 100µm ($L=12\lambda$) in width, resulting in a figure of merit FoM (FOM= $k_t^2.Q$) of 87. This performance surpasses the current existing technologies (Table I) designed to operate in the same frequency range.

TABLE I. Performance comparison between state-of-art piezoelectric micro-resonators.

State of art	f_r (GHz)	k_t^2	Q	FOM	ref
AlN-LOBAR	1	1%	3891	39	[17]
AlN-LFE	2,8	2,5%	1855	45	[18]
$LiNbO_3$-LFE	0,5	11,5%	362	41	[19]
This work	**0,7**	**7,4%**	**1180**	**87**	

f_r is the resonance frequency
k_t^2 is the electromechanical coupling coefficient
Q is the quality factor
FOM is the figure of merit
LOBAR: lateral overtone bulk acoustic resonator
LFE: Lateral field excitation

C. Evolution of device's quality factor with different ZnO thicknesses

A group of three resonator devices with three different thicknesses of ZnO (200 nm, 600 nm and 800 nm) were fabricated and tested.

The three devices were designed with the same number of IDTs ($n=80$) and length ($L=25\lambda$). Measurement results are shown in Figure 11. The resonance frequency response of the micro-resonators decreases from 765 MHz down to 672 MHz with increasing the ZnO thickness from 200 nm to 800 nm. These results were somehow expected since the composite ZnO/Si composite layer thickness is increasing and the resonant frequency value of the device is inversely proportional to its thickness [20]. It can be seen that an excellent agreement is obtained between the MBVD model and the measured results, clearly showing the validity of Q extraction using the equivalent electrical circuit.

The FEM simulations were employed for predicting the vibration frequencies of the ZnO micro-resonators. The measured and simulated results of resonant frequency and Q for resonators incorporating ZnO layers with thicknesses from 200 nm to 1000 nm are represented in Table II. A discrepancy of less than 4% was found between the FEM analysis and experimental data, further proving that the actual behavior of these micro-resonators can be described by conventional models. Figure 12 present a comparison of the calculated $f.Q$ product between measured and simulated results. From the results presented in table 2 we can notice that decreasing ZnO thickness increases the quality factor from 430 (for the 800 nm thick ZnO layer) to 1600 (for the 200 nm thick ZnO). This behavior can be explained by the fact that thin ZnO layers allow to take full benefit of the very high quality factor of the single crystal silicon membrane. However, reducing the ZnO thickness to less than 200 nm would results in poor-crystalline ZnO layers with modest piezoelectric properties.

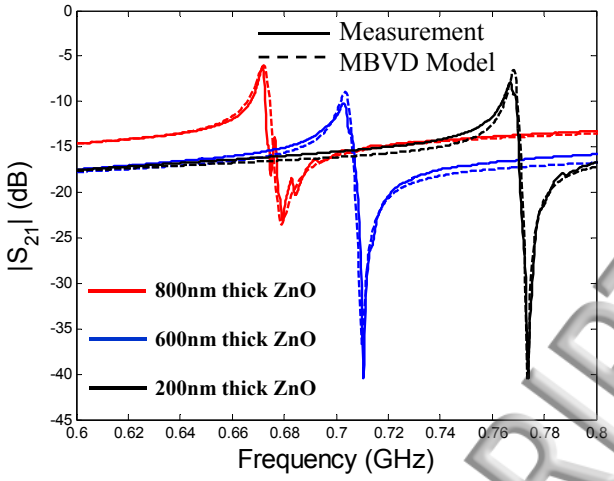

FIG. 11. Measured and simulated transmission response of fabricated ZnO resonators with different ZnO thicknesses

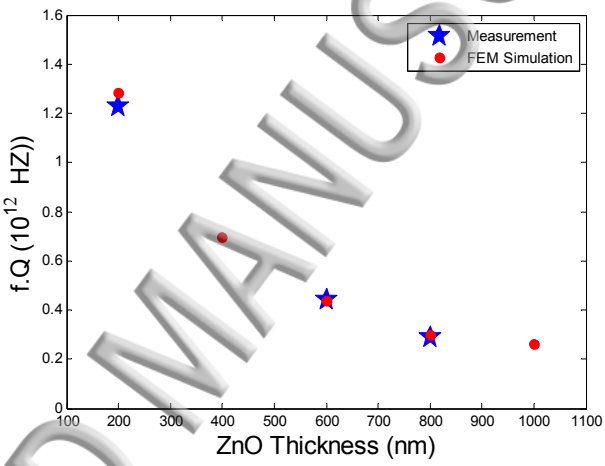

FIG. 12. Simulated and measured evolution of $f.Q$ product for the three tested thicknesses of ZnO.

TABLE II. Comparison between simulated and measured values of the resonance frequency f_r and the quality factor Q.

	Resonance Frequency f_r (MHz)		*Quality factor Q*	
ZnO thickness (nm)	Measurement	FEM Simulation	Measurement	FEM Simulation
200	765	767	1600	1675
400	-	727	-	955
600	703	705	618	635
800	672	679	430	450
1000	-	657	-	400

The results presented so far clearly show that thin ZnO layers on Si membranes are well suited for the fabrication of high Q resonators.

V. POWER HANDLING AND NONLINEAR CHARACTERIZATION OF SINGLE MICRO-RESONATORS

The power-handling capability and nonlinear behavior of the ZnO micro-resonators were experimentally investigated by measuring the transmission response at various input power levels. The input power was swept from 5 to 22 dBm. We visually noticed that by increasing the input power, the suspend resonators were subject to mechanical vibrations. These vibrations were amplified by applying large electric fields to the piezoelectric layer especially at the resonance frequency, so the input power level was limited to 22 dBm in order to protect the probing high-frequency pads.

A. Set-up

Figure 13 presents the set-up used for power characterization of the micro-resonators [21]. We use the ZVA 24 GHz analyzer to generate a poser RF signal at port 1 and we monitor the transmitted power signal at port 2.

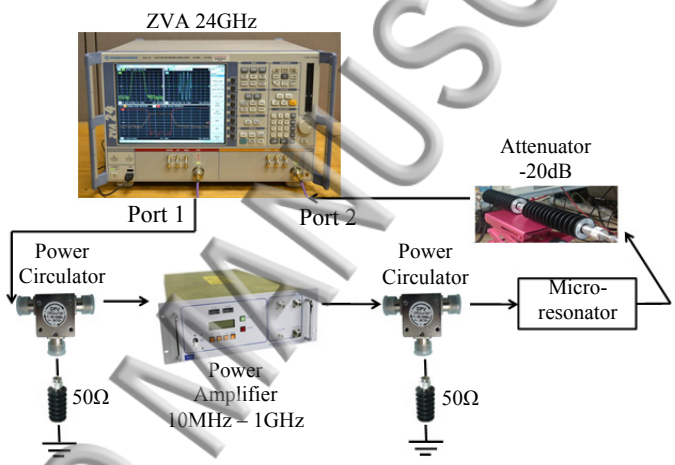

FIG. 13. Set-up characterization of micro-resonators for high RF power level.

A power amplifier (PA) EM Power between 10 MHz and 1 GHz is used for amplifying the input RF signal by 43 dBm. Two power circulators with third port connected to a load of 50 ohms are introduced before the PA and after the ZVA analyzer output port 1 to protect them from reflected power from the device. An attenuator is placed before the ZVA input port 2 to protect it from the high power circulating in the characterization chain. A “transmission response” calibration is realized at a power level of 18 dBm before measurement to correct the errors of the transmission response.

B. Power handling in micro-resonators

Two examples of power sweep measurement are shown in Figure 14. This test is realized to find the bifurcation point which can be considered as the highest level of power that the device can handle before large nonlinearity is recorded. It is also defined as the input power at which magnitude shows a vertical slope in amplitude and displays the verge of instability [22].

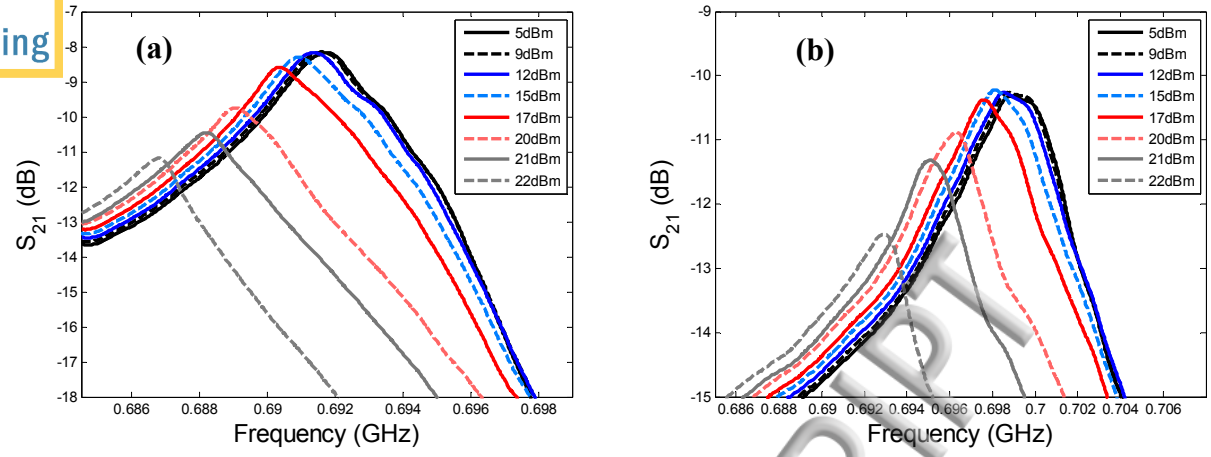

FIG. 14. Frequency response around 700 MHz of two micro-resonators for different injected different power levels: (a) *n=40* & *L=12λ,* (b) *n=40* & *L=17λ*.

Looking at Figure 14, we mention that the nonlinear changes are confined around this frequency where we may notice a severe frequency shift for f_r of 5 MHz with increasing the input power. In the frequency regions out-side the resonant frequency area, the piezoelectric layer is not in the resonance mode and behaves as a static capacitance depending on the permittivity of the material (ZnO): we do not noticed any dielectric change with S-parameters measurements so the ZnO's permittivity ε_{33} is constant.

The power handling test was realized for three micro-resonators with the same number of IDTs *n=40* (this number is chosen because of the very high quality factor, as demonstrated in part 3) but different lengths (12λ, 17λ and 25 λ). As shown in Figure 14, for the presented two micro-resonators, the resonance peaks are slightly bend at the maximum power (22 dBm) but no bifurcation point is detected. This is a very unique situation where a suspended micro-resonator can support 22 dBm without breaking and also without any bifurcation point. The low resistivity of SOI wafers employed for device fabrication may explain these results. It was demonstrated in [22] that for similar micro-resonators fabricated on high doping level of silicon substrate (which result in a low resistivity) are less susceptible to be driven to nonlinearity compared to higher doped wafers. Insertion losses remain stable until 14 dBm and increase after this power level.

In order to analyze the nonlinearity degree of these devices, we define a normalized frequency shift S_N which is calculated as the difference between the shifted peak frequency (f_s) and the center frequency (f_r) divided by f_s [23]:

$$S_N = \frac{f_s - f_r}{f_s} \tag{4}$$

The nonlinearity behavior can be detected when S_N takes a value different of zero. Figure 15 shows that the nonlinearity begins at lower power level when micro-resonators have small IDTs. The power level dependence of S_N can be separated into two zones. In the first one between 5 dBm and 20 dBm, the micro-resonator with higher IDTs lengths has a smaller S_N than

that having lower IDTs lengths. Clearly, the micro-resonator with lower IDTs lengths becomes nonlinear at a lower injected power. By increasing the power, in the 20 dBm- 22dBm domain, micro-resonators converge to the same S_N value. This imply that for power levels lower than 20 dBm micro-resonator devices with longer IDTs are able to support more power before beginning to shift in frequency but these three devices (irrespective of their IDTs length) converge to the same S_N values after 20 dBm.

So we can deduce that between 5 dBm and 20 dBm, the frequency shift behavior is related to the length of the IDTs: micro-resonators with lower IDTs lengths become nonlinear at a lower injected power. After 20 dBm of injected power, micro-resonators converge to the same S_N value, probably because the nonlinear phenomena are becoming more sensitive to the thickness of ZnO layer and Si membrane, which are the same in all tested micro-resonators.

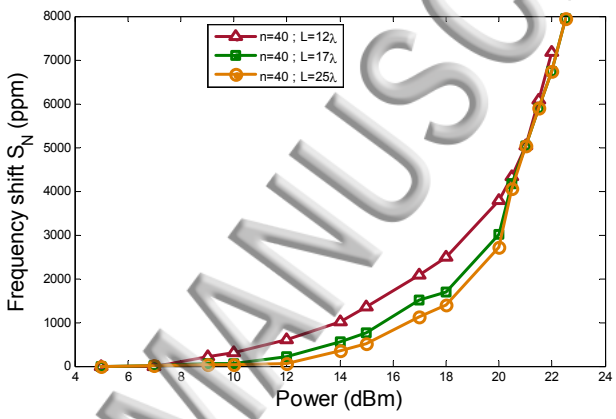

FIG. 15. The normalized frequency shift (S_N) as a function of delivered power for two different combinations of micro-resonators operating around 700MHz.

Our results show that ZnO-based micro-resonators can handle high power levels. This is a clear evidence of the fact that the piezoelectric micro-resonators technology can be advantageously used for high power applications.

VI. TEMPERATURE STABILITY

The frequency-temperature characteristic (TCF) of ZnO micro-resonators was also measured in the temperature range from 293 to 363 K. The temperature was varied in 10 K increments and the S-parameters measurements were performed after a 5 minute period of temperature stabilization.

Two micro-resonators with different IDTs number and lengths were tested: first one with $n=25$ & $L=21\lambda$ and the second one with $n=40$ & $L=12\lambda$. The resonant frequency variation with temperature of one of a measured micro-resonator response is presented in Figure 16.

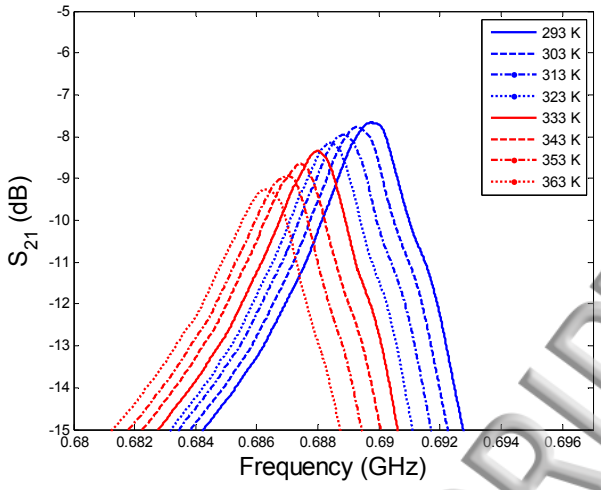

FIG. 16. Transmission response around the resonant frequency of a fabricated micro-resonator measured in the temperature range from 293 to 363K.

This variation is mainly caused by the dependence of the acoustic velocity on temperature. The acoustic velocity is determined by $(E/\rho)^{1/2}$, where E and ρ are the Young's modulus and mass density, respectively. For ZnO, Young's modulus and the mass density decreases as temperature increases due to the material softening. The dominant effect on the Young's modulus result in decreasing of the acoustic velocity as temperature increases, resulting in a negative TCF (resonant frequency decreasing with increasing temperature).

To extract the device TCF, the resonant frequency shift with temperature is shown in Figure 17 for both micro-resonators and fitted with a linear equation. Both micro-resonators show approximately the same TCF (64.72 ppm/K and 65.7 ppm/K). These values are near to the TCF of a conventional ZnO FBAR device (−70 ppm/°C) demonstrated in [24].

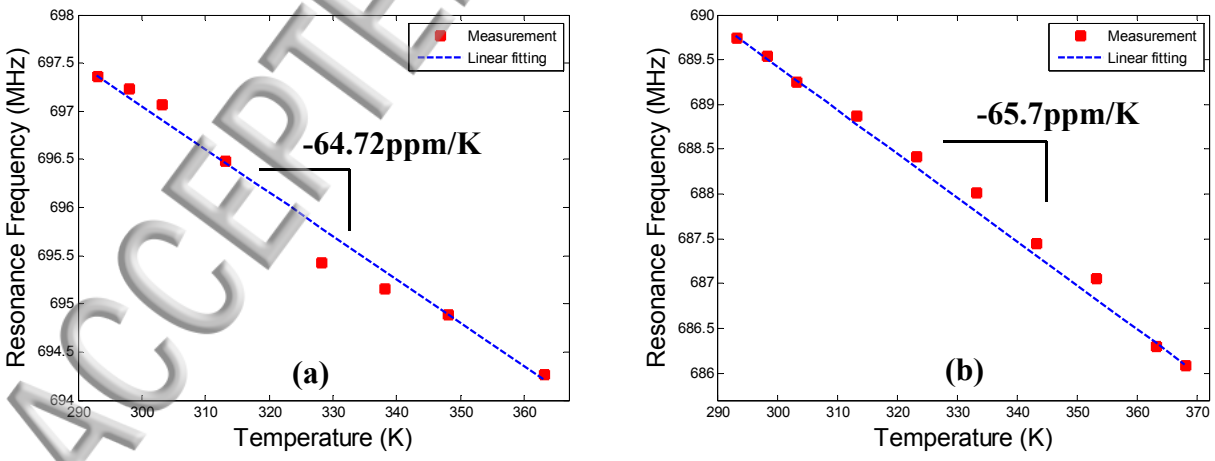

FIG. 17. The frequency shift with temperature measured and fitted with linear equation for two micro-resonators: (a) *n=25* & *L=21λ*, (b) *n=40* & *L=12λ*

VII. CONCLUSION

In this paper, we report the design, simulation, fabrication and test results of piezoelectric ZnO-based contour-mode micro-resonators. We have demonstrated that spurious modes which are in close proximity of the main mechanical resonance frequency are the principle cause in decreasing performances of suspended ZnO micro-resonators. These modes are associated with the large number of IDTs electrodes and decrease the quality factor of the devices. To study the impact of spurious modes on micro-resonators Q and k_t^2 we varied the geometry of IDTS electrodes (n and L) while keeping the size of the vibrating body fixed.

The optimization on the ZnO layer thickness allowed obtaining a high $f.Q$ product $\approx 1{,}23\times10^{12}$ Hz around 765 MHz, with a high unloaded quality factors (Q) up to 1600 which prove that thin piezoelectric transducer layers enhances the quality factor. In addition, the optimization of n and L allowed obtaining a very high electromechanical coupling coefficient k_t^2 of 7.4% with a high quality factor Q equal to 1180 have been achieved by mechanically coupling 40- electrodes type IDTs of 100 µm ($L=12\lambda$) in width which allowed achieving a very high figure of merit (FOM= $k_t^2.Q$) of 87.

Future work will focus on increasing the operating frequency of the micro-resonators towards GHz frequencies domain. Also, the demonstration of complex filtering functions using this technology will be very interesting. Finally, these devices can be used to fabricate sensors because of their high piezoelectric sensibility especially in term of temperature as we saw.

SUPLEMENTARY MATERIAL

See supplementary material for more information concerning: X-ray diffraction curve of ZnO thin films deposited on molybdenum film (presented in part II), the used MBVD model (presented in part III) and values of extracted electrical components of MBVD model (presented in part IV).

REFERENCES

[1]R. Aigner, "SAW and BAW technologies for RF filter applications: A review of the relative strengths and weaknesses," *2008 IEEE Ultrasonics Symposium*, Beijing, 2008, pp. 582-589.

[2]A. Reinhardt, G. Parat, E. Defaÿ, M. Aïd and F. Domingue, "Acoustic technologies for advanced RF architectures," *NEWCAS Conference (NEWCAS), 2010 8th IEEE International*, Montreal, QC, 2010, pp. 161-164.

[3]R. Ruby, P. Bradley, D. Clark, D. Feld, T. Jamneala and Kun Wang, "Acoustic FBAR for filters, duplexers and front end modules," *Microwave Symposium Digest, 2004 IEEE MTT-S International*, 2004, pp. 931-934 Vol.2.

[4]Rinaldi, M.; Zuniga, C.; Piazza, G., "5-10 GHz AlN Contour-Mode Nanoelectromechanical Resonators," Micro Electro Mechanical Systems, 2009. MEMS 2009. IEEE 22nd International Conference on, pp.916, 91, 25-29 Jan. 2009.

[5]R. Lanz and P. Muralt, "Solidly mounted BAW filters for 8 GHz based on AlN thin films," *Ultrasonics, 2003 IEEE Symposium on*, 2003, pp. 178-181 Vol.1.

[6]Flament, A. Frappe, B. Stefanelli, A. Kaiser, A. Cathelin, S. Giraud, M. Chatras, S. Bila, D. Cros, J.B. David, L. Leyssenne, E. Kerhervé. "A complete UMTS transmitter using BAW filters and duplexer, a 90nm CMOS digital RF signal generator and a 0.25µm BiCMOS power amplifier", International Journal of RF and Microwave Computer-Aided Engineering, september 2011, Vol 21, Issue 5, pp 466-476.

[7]L. Catherinot, S. Giraud, M. Chatras, S. Bila, D. Cros, T. Baron, S. Ballandras, P. Monfraix, L. Estagerie "A general procedure for the desing of BAW filters", International Journal of RF and Microwave Computer-Aided Engineering, September 2011, Vol 21, Issue 5, pp 458-465

[8]S. Giraud, S. Bila, M. Chatras, D. Cros and M. Aubourg, "Bulk acoustic wave filters synthesis and optimization for multi-standard communication terminals," in *IEEE Transactions on Ultrasonics, Ferroelectrics, and Frequency Control*, vol. 57, no. 1, pp. 52-58, Jan. 2010.

[9]J. Liu, J. Liu, S. Li, S. He, Y. Liang and H. Li, "Switchable low loss SAW filter bank with SAW notch filters," *2008 IEEE Ultrasonics Symposium*, Beijing, 2008, pp. 1600-1602.

[10]X. Lu, J. Galipeau, K. Mouthaan, E. H. Briot and B. Abbott, "Reconfigurable multiband SAW filters for LTE applications," *2013 IEEE Radio and Wireless Symposium*, Austin, TX, 2013, pp. 253-255.

[11]M. Ossama, B. Pierre, C. Aurelian, C. Matthieu and J. C. Orlianges, "A zinc dioxide-on-silicon MEMS resonator for narrowband filtering," *Electronics, Circuits and Systems (ICECS), 2014 21st IEEE International Conference on*, Marseille, 2014, pp. 586-589.

[12]Shi, L.; Piazza, G., "Lithium Niobate on Silicon Dioxide Suspended Membranes: A Technology Platform for Engineering the Temperature Coefficient of Frequency of High Electromechanical Coupling Resonators," in Microelectromechanical Systems, Journal of, vol.23, no.6, pp.1318-1329, Dec. 2014.

[13]Chengjie Zuo, Nipun Sinha, Gianluca Piazza, "Very high frequency channel-select MEMS filters based on self-coupled piezoelectric AlN contour-mode resonators", Sensors and Actuators A: Physical, Volume 160, Issues 1–2, May 2010, Pages 132-140.

[14]M. Chatras, P. Blondy, D. Cros, O. Vendier and J. L. Cazaux, "A surface-mountable membrane supported filter," in *IEEE Microwave and Wireless Components Letters*, vol. 13, no. 12, pp. 535-537, Dec. 2003.

[15]Petersen, K.E., "Silicon as a mechanical material," Proceedings of the IEEE, vol.70, no.5, pp.420, 457, May 1982.

[16]Wanling Pan, R. Abdolvand and Farrokh Ayazi, "A low-loss 1.8GHz monolithic thin-film piezoelectric-on-substrate filter," *Micro Electro Mechanical Systems, 2008. MEMS 2008. IEEE 21st International Conference on*, Tucson, AZ, 2008, pp. 176-179.

[17]N. K. Kuo et al., "Micromachined sapphire GHz lateral overtone bulk acoustic resonators transduced by aluminum nitride," 2012 IEEE 25th International Conference on Micro Electro Mechanical Systems (MEMS), Paris, 2012, pp. 27-30

[18]Y. Hui, Z. Qian and M. Rinaldi, "A 2.8 GHz combined mode of vibration aluminum nitride MEMS resonator with high figure of merit exceeding 45," 2013 Joint European Frequency and Time Forum & International Frequency Control Symposium (EFTF/IFC), Prague, 2013, pp. 930-932

[19]S. Gong and G. Piazza, "Design and Analysis of Lithium–Niobate-Based High Electromechanical Coupling RF-MEMS Resonators for Wideband Filtering," in IEEE Transactions on Microwave Theory and Techniques, vol. 61, no. 1, pp. 403-414, Jan. 2013.

[20]Wanling Pan and F. Ayazi, "Multiple-frequency thickness-mode thin-film piezoelectric-on-substrate filter array," *2008 IEEE International Frequency Control Symposium*, Honolulu, HI, 2008, pp. 259-262.

[21]W. Sahyoun, J. M. Duchamp and P. Benech, "Nonlinear behavior of AlN in BAW and CRF devices for high RF electric field," *Microwave Integrated Circuits Conference (EuMIC), 2011 European*, Manchester, 2011, pp. 426-429.

[22]M. Shahmohammadi, H. Fatemi and R. Abdolvand, "Nonlinearity reduction in silicon resonators by doping and re-orientation," *Micro Electro Mechanical Systems (MEMS), 2013 IEEE 26th International Conference on*, Taipei, 2013, pp. 793-796.

[23]M. Shahmohammadi, B. P. Harrington and R. Abdolvand, "Concurrent enhancement of Q and power handling in multi-tether high-order extensional resonators," *Microwave Symposium Digest (MTT), 2010 IEEE MTT-S International*, Anaheim, CA, 2010, pp. 1452-1455.

[24]H. Yu, W. Pang, H. Zhang and E. S. Kim, "Ultra Temperature-Stable Bulk-Acoustic-Wave Resonators with SiO2 Compensation Layer," in *IEEE Transactions on Ultrasonics, Ferroelectrics, and Frequency Control*, vol. 54, no. 10, pp. 2102-2109, October 2007.

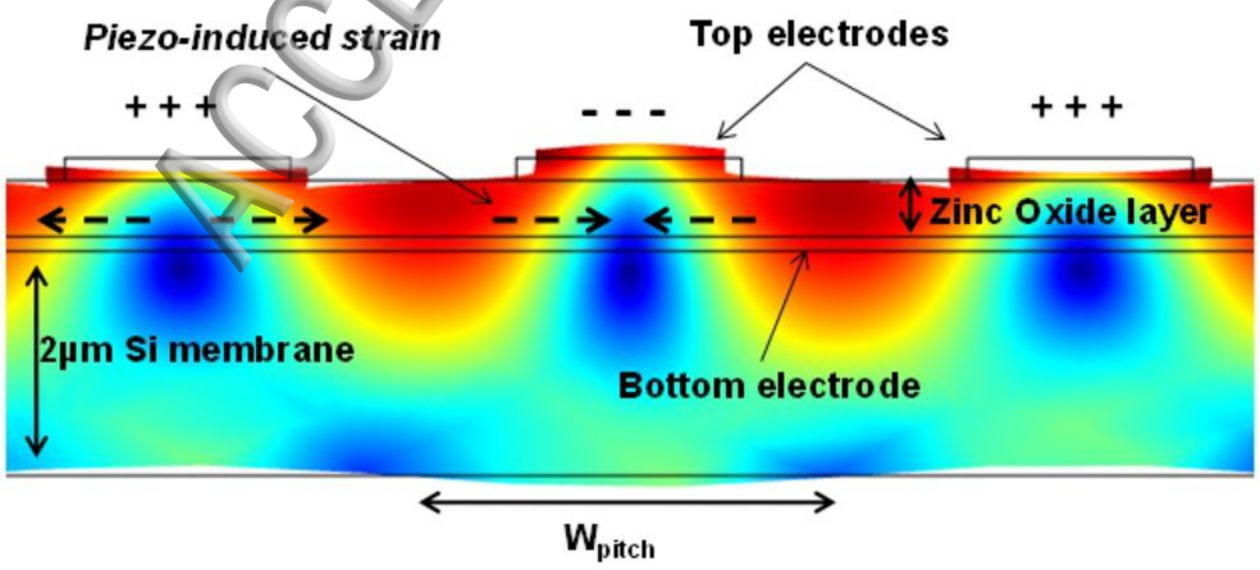
Piezo-induced strain
Top electrodes
+ + +
- - -
+ + +
Zinc Oxide layer
2µm Si membrane
Bottom electrode
W_{pitch}

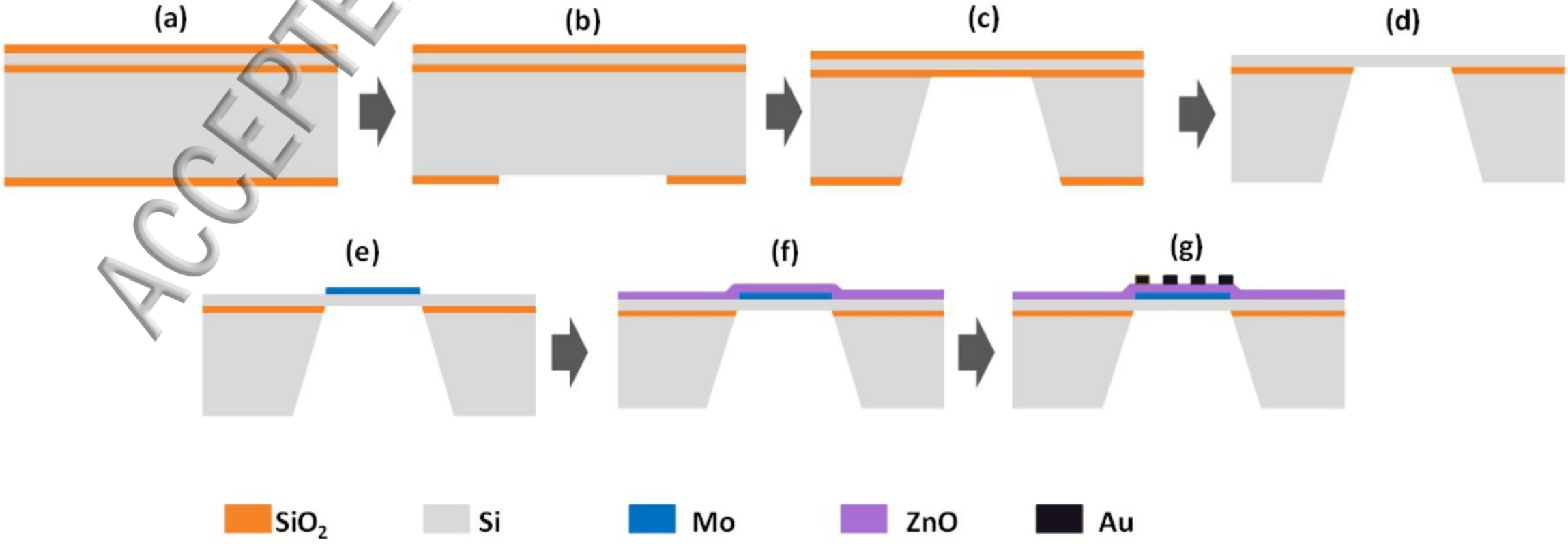

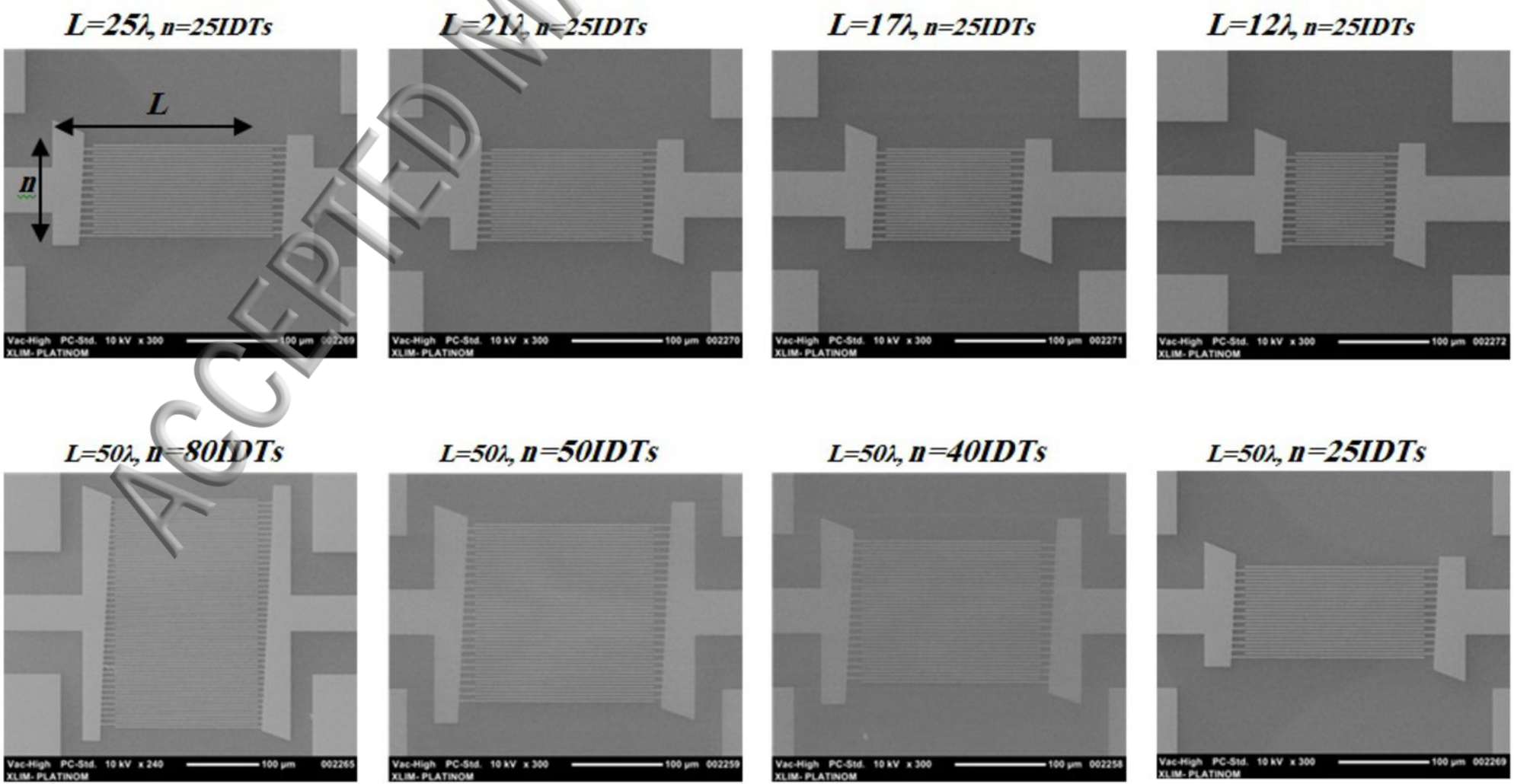
L=25λ, n=25IDTs
L=21λ, n=25IDTs
L=17λ, n=25IDTs
L=12λ, n=25IDTs
L
n
L=50λ, n=80IDTs
L=50λ, n=50IDTs
L=50λ, n=40IDTs
L=50λ, n=25IDTs

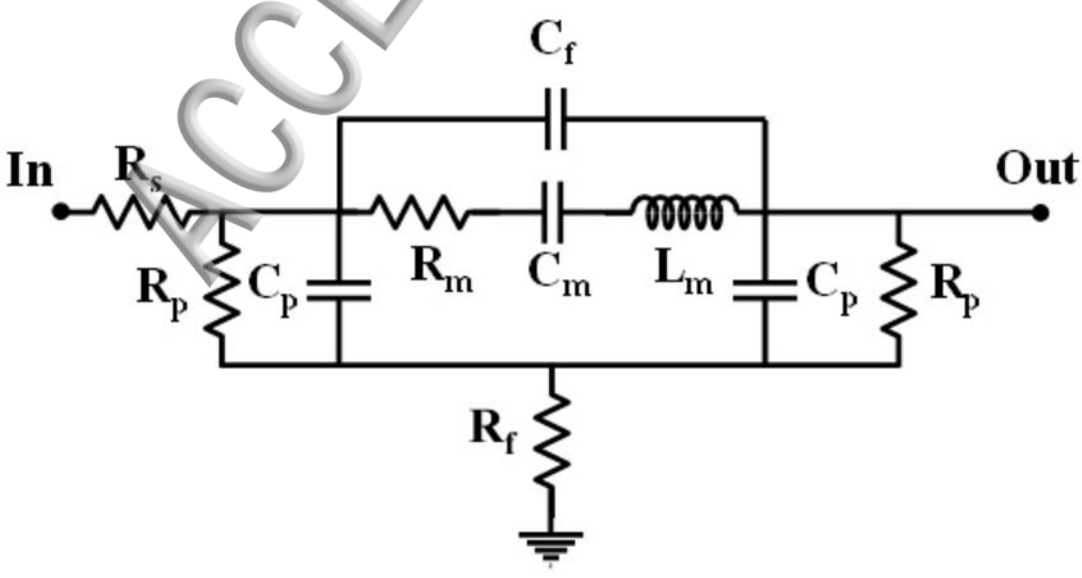
C_f
In
R_s
Out
R_p
C_p
R_m
C_m
L_m
C_p
R_p
R_f

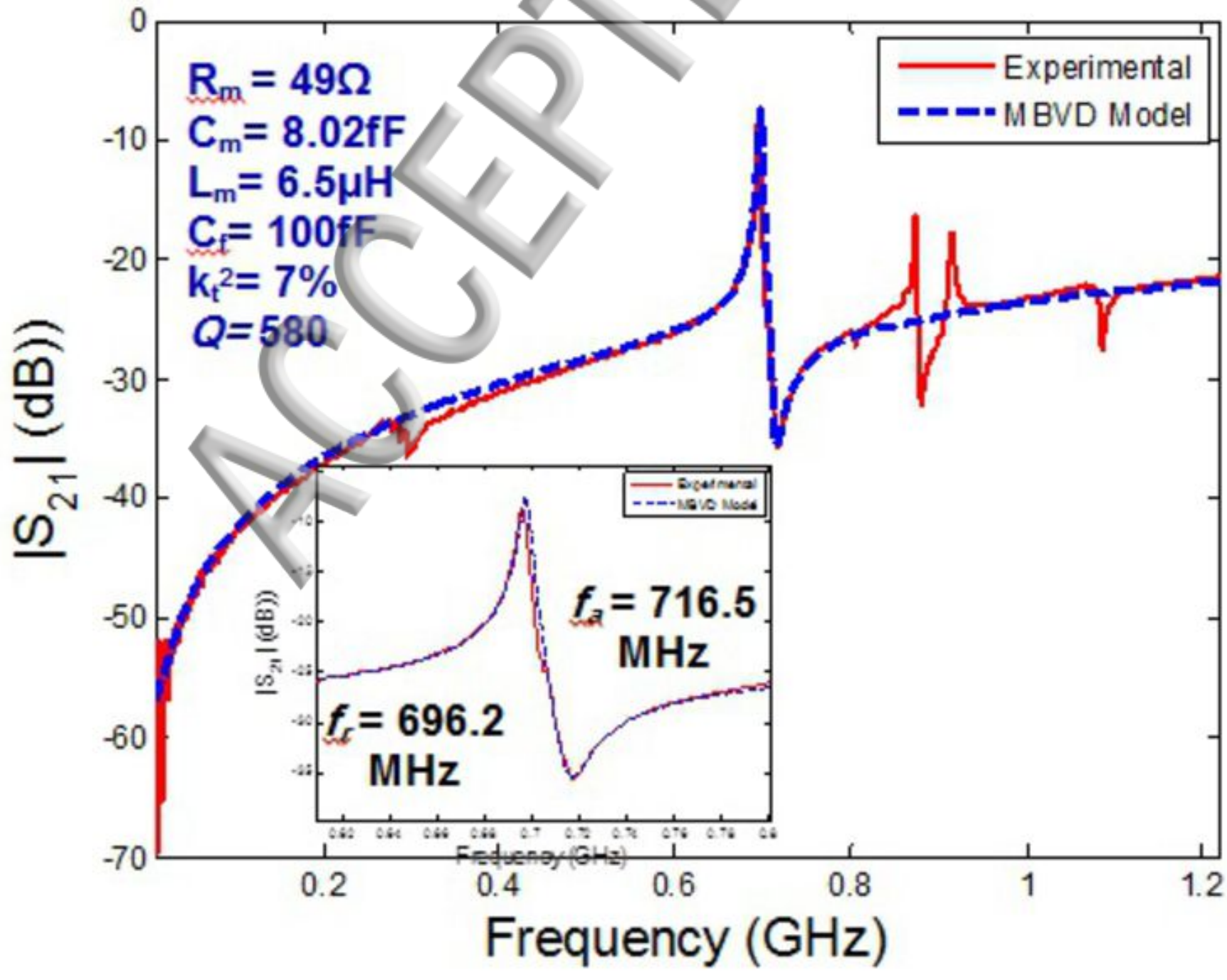
R_m = 49Ω
C_m= 8.02fF
L_m= 6.5μH
C_t= 100fF
k_t^2= 7%
Q=580
Experimental
MBVD Model
$|S_{21}|$ (dB))
Frequency (GHz)
f_a = 716.5 MHz
f_r = 696.2 MHz

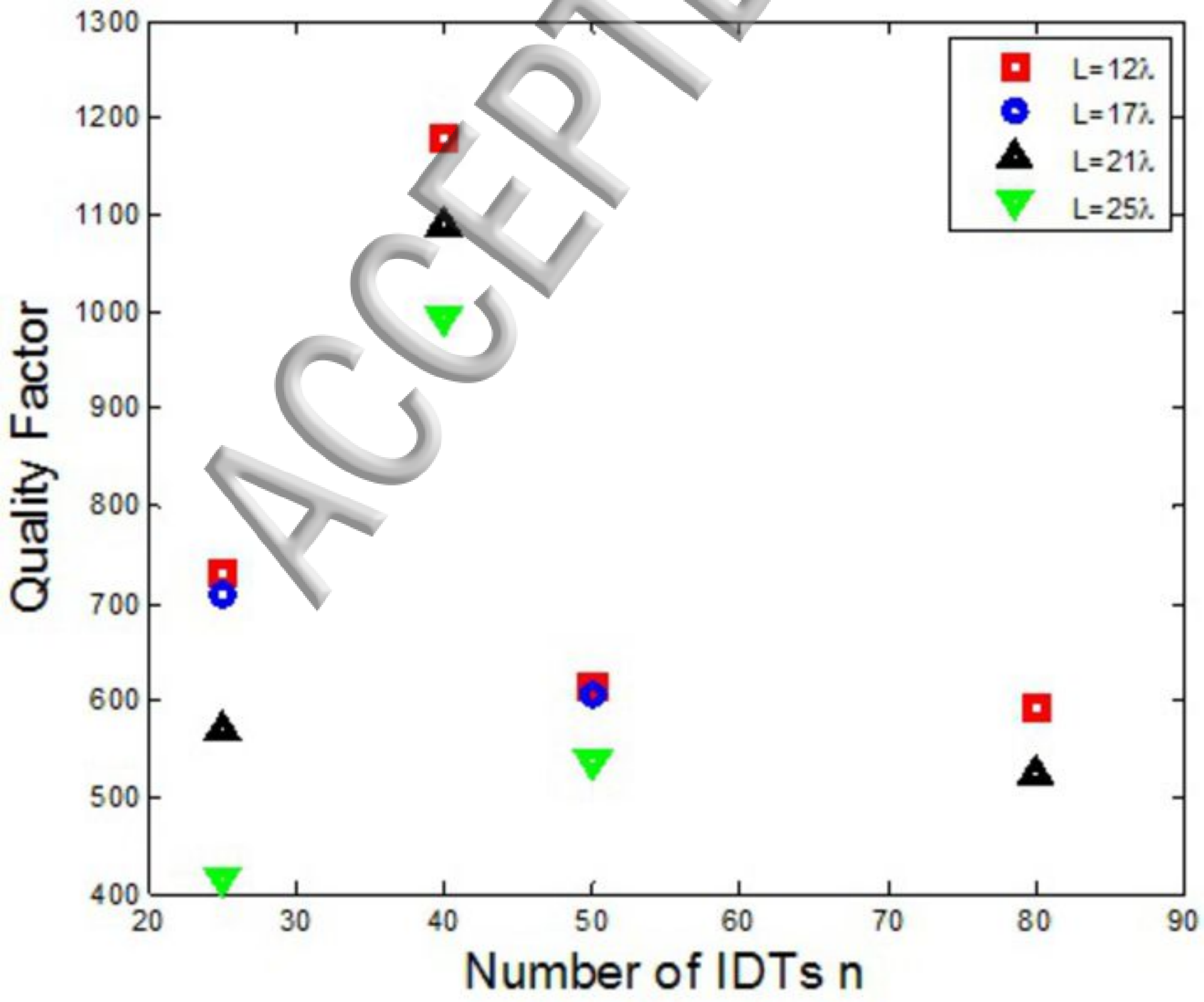
Quality Factor
Number of IDTs n
L=12λ
L=17λ
L=21λ
L=25λ
1300
1200
1100
1000
900
800
700
600
500
400
20
30
40
50
60
70
80
90

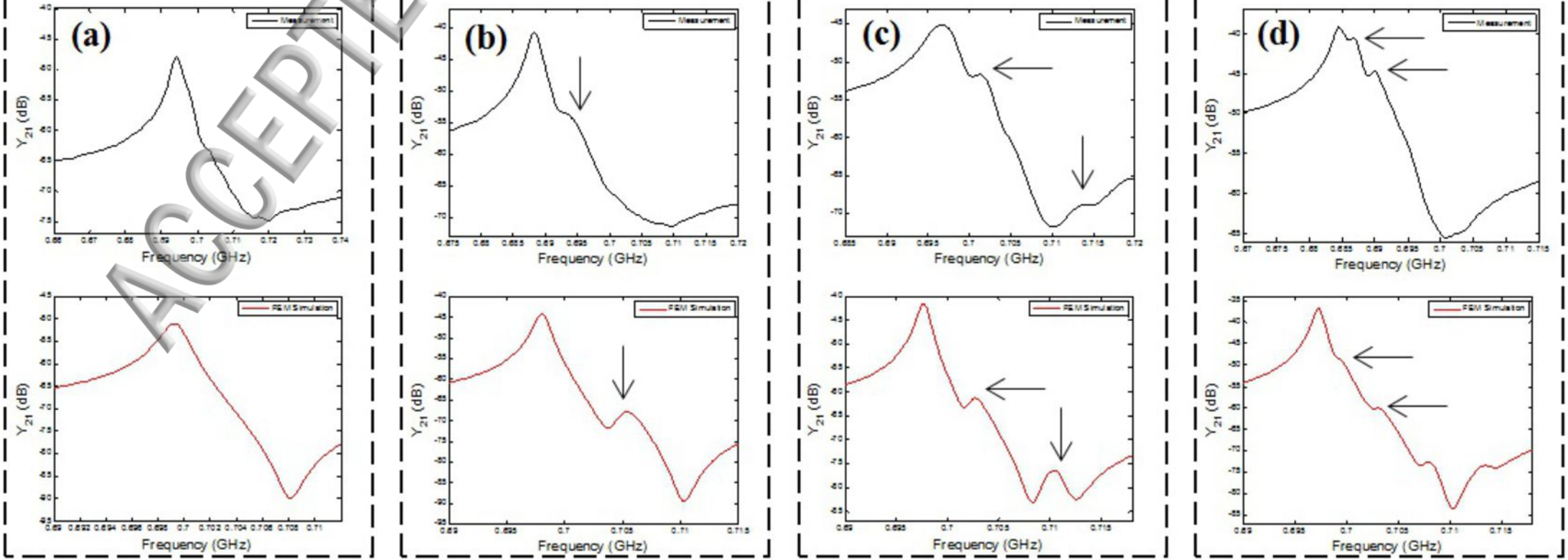

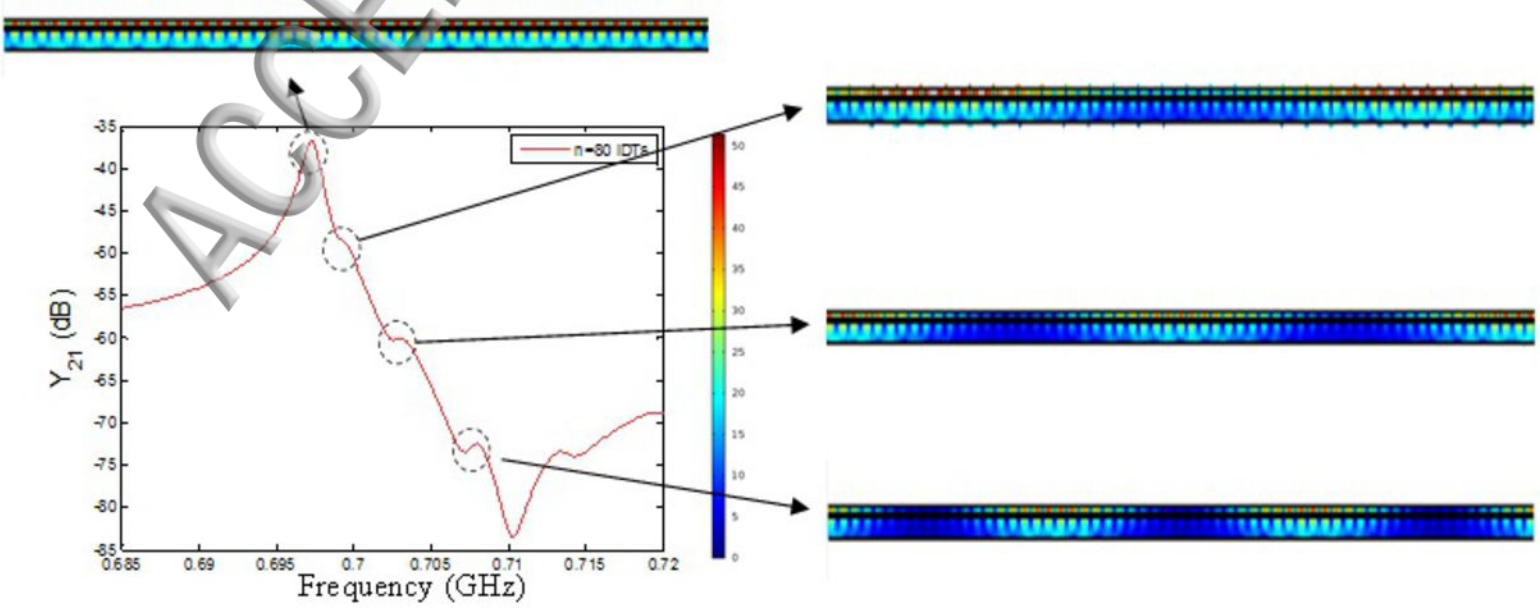
n=80 IDTs
Y21 (dB)
Frequency (GHz)
-35
-40
-45
-50
-55
-60
-65
-70
-75
-80
-85
0.685
0.69
0.695
0.7
0.705
0.71
0.715
0.72
50
45
40
35
30
25
20
15
10
5
0

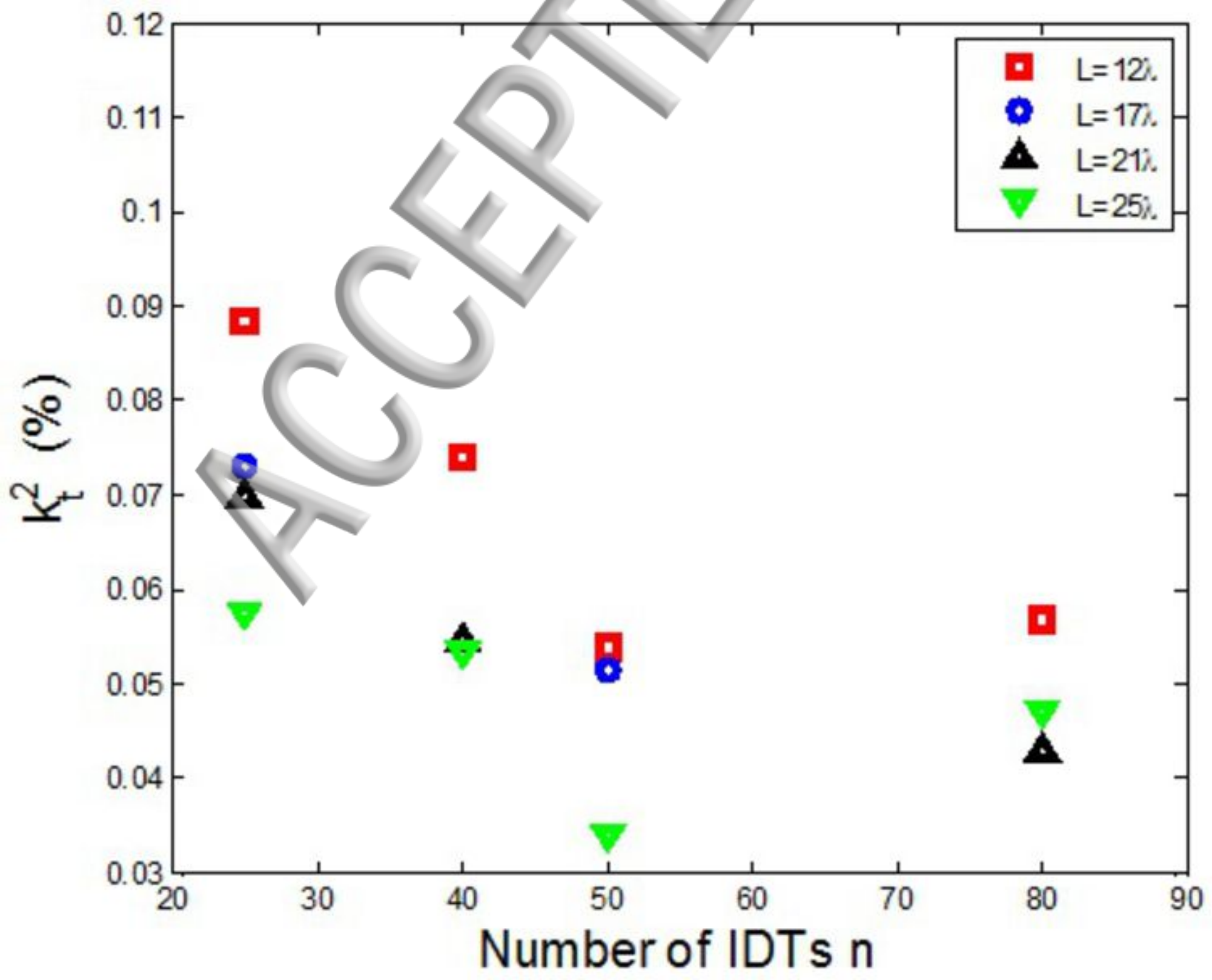
0.12
0.11
0.1
0.09
0.08
0.07
0.06
0.05
0.04
0.03
k_t^2 (%)
20
30
40
50
60
70
80
90
Number of IDTs n
L=12λ
L=17λ
L=21λ
L=25λ

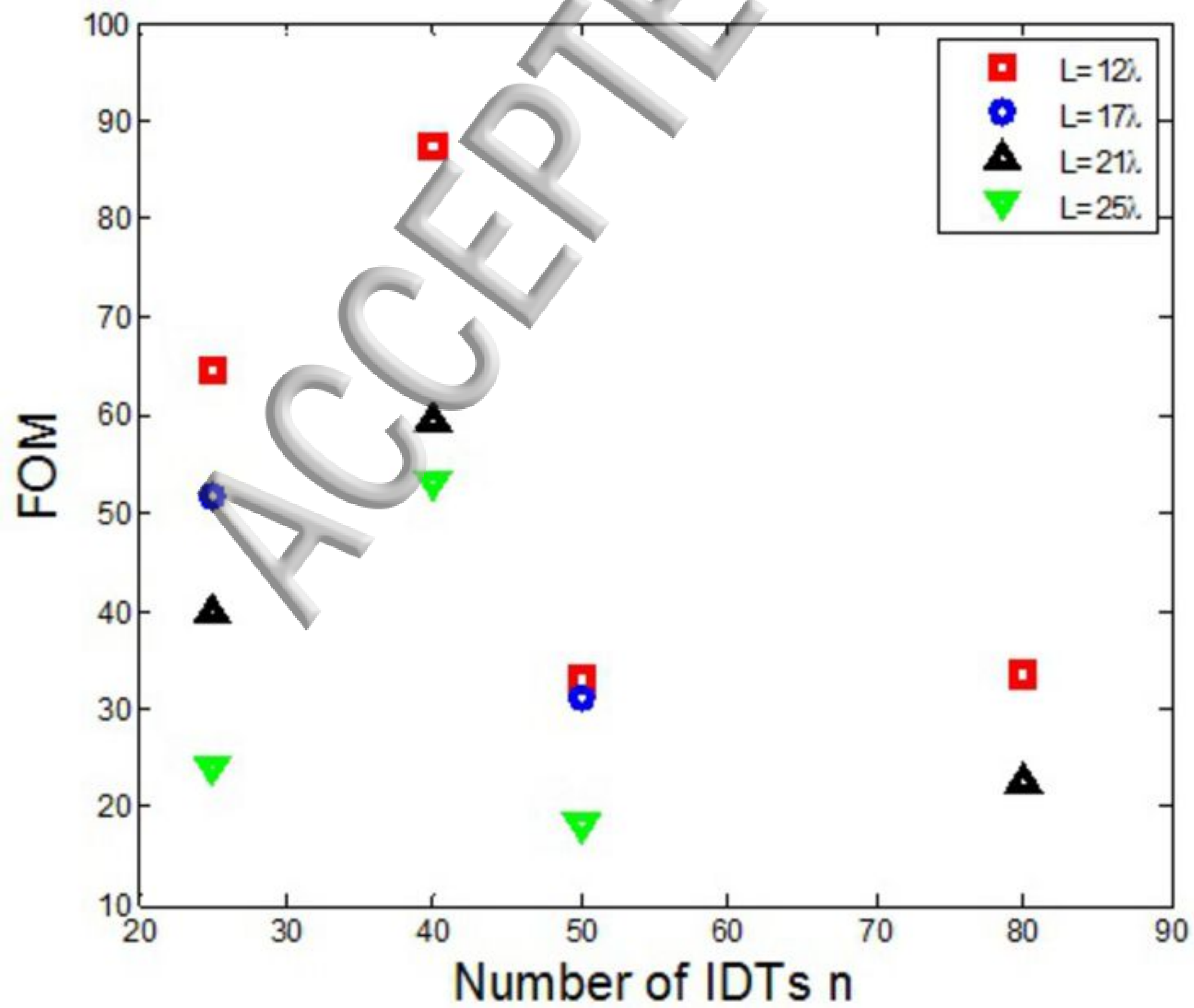
FOM
Number of IDTs n
L=12λ
L=17λ
L=21λ
L=25λ
100
90
80
70
60
50
40
30
20
10
20
30
40
50
60
70
80
90

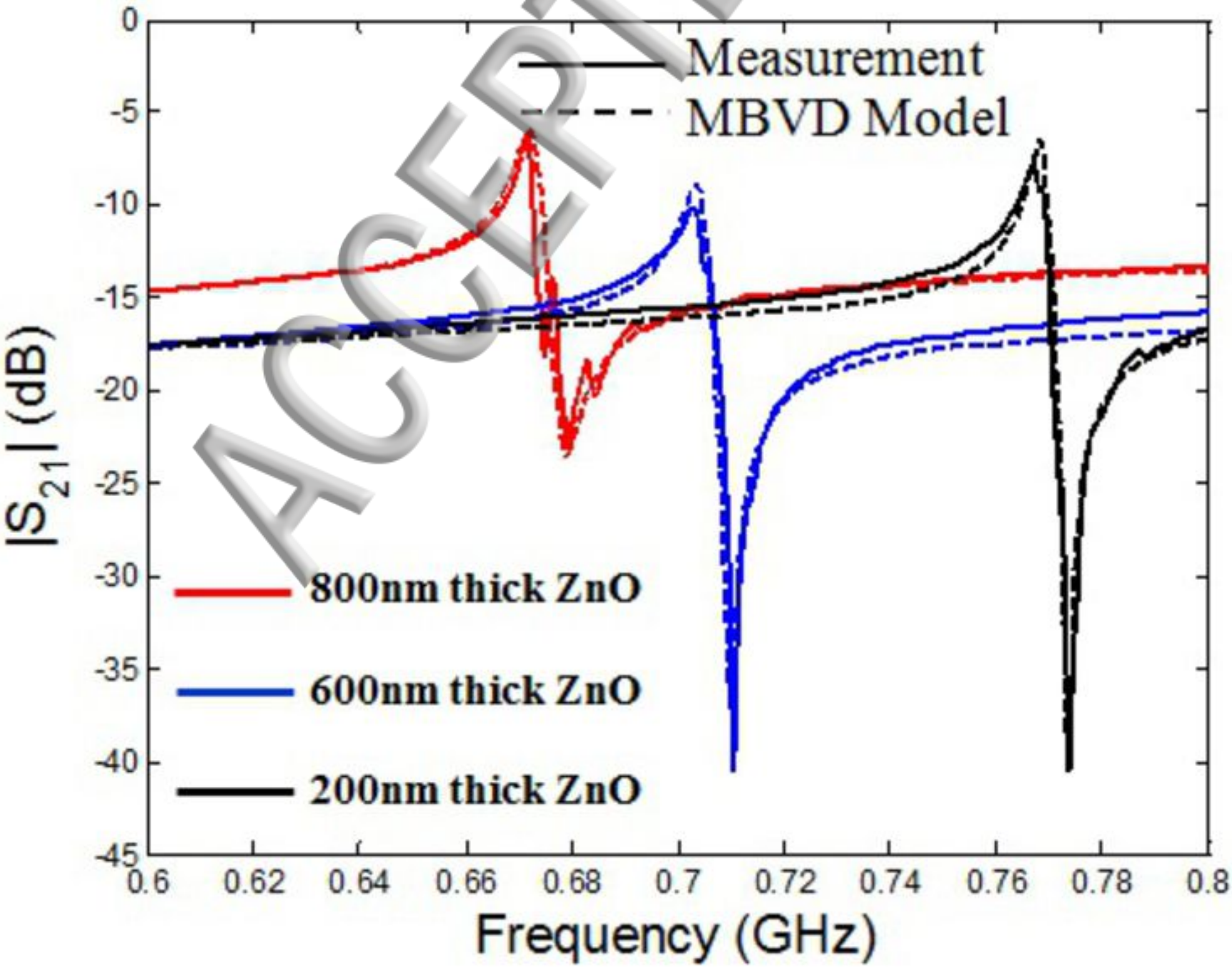
Measurement
MBVD Model
800nm thick ZnO
600nm thick ZnO
200nm thick ZnO
|S21| (dB)
Frequency (GHz)
0
-5
-10
-15
-20
-25
-30
-35
-40
-45
0.6
0.62
0.64
0.66
0.68
0.7
0.72
0.74
0.76
0.78
0.8

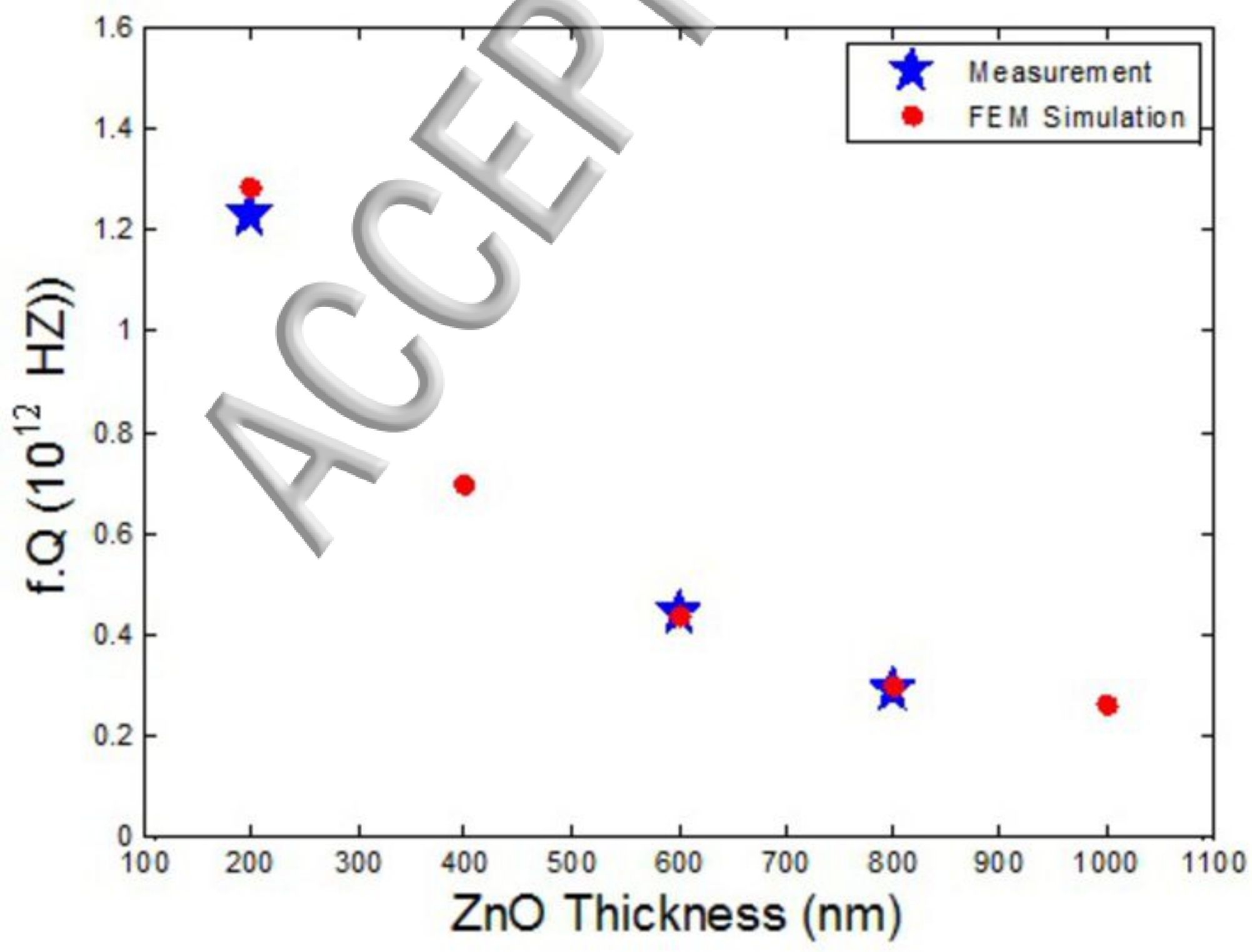
Measurement
FEM Simulation
f.Q (10^12 HZ))
ZnO Thickness (nm)
0
0.2
0.4
0.6
0.8
1
1.2
1.4
1.6
100
200
300
400
500
600
700
800
900
1000
1100

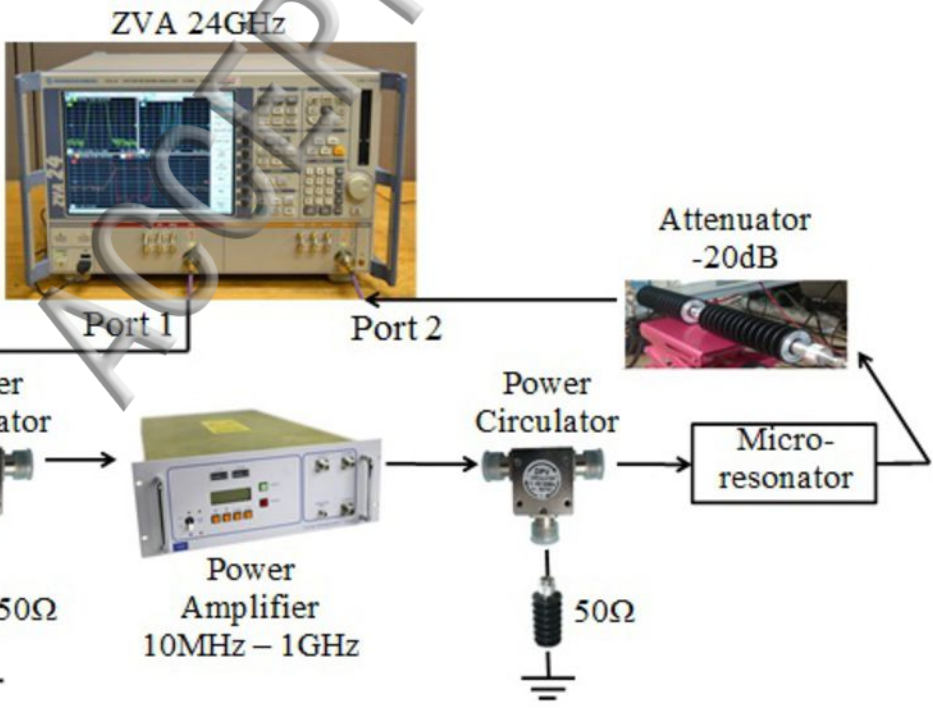
ZVA 24GHz
Attenuator
-20dB
Port 1
Port 2
Power
Circulator
Power
Circulator
Micro-
resonator
50Ω
Power
Amplifier
10MHz – 1GHz
50Ω

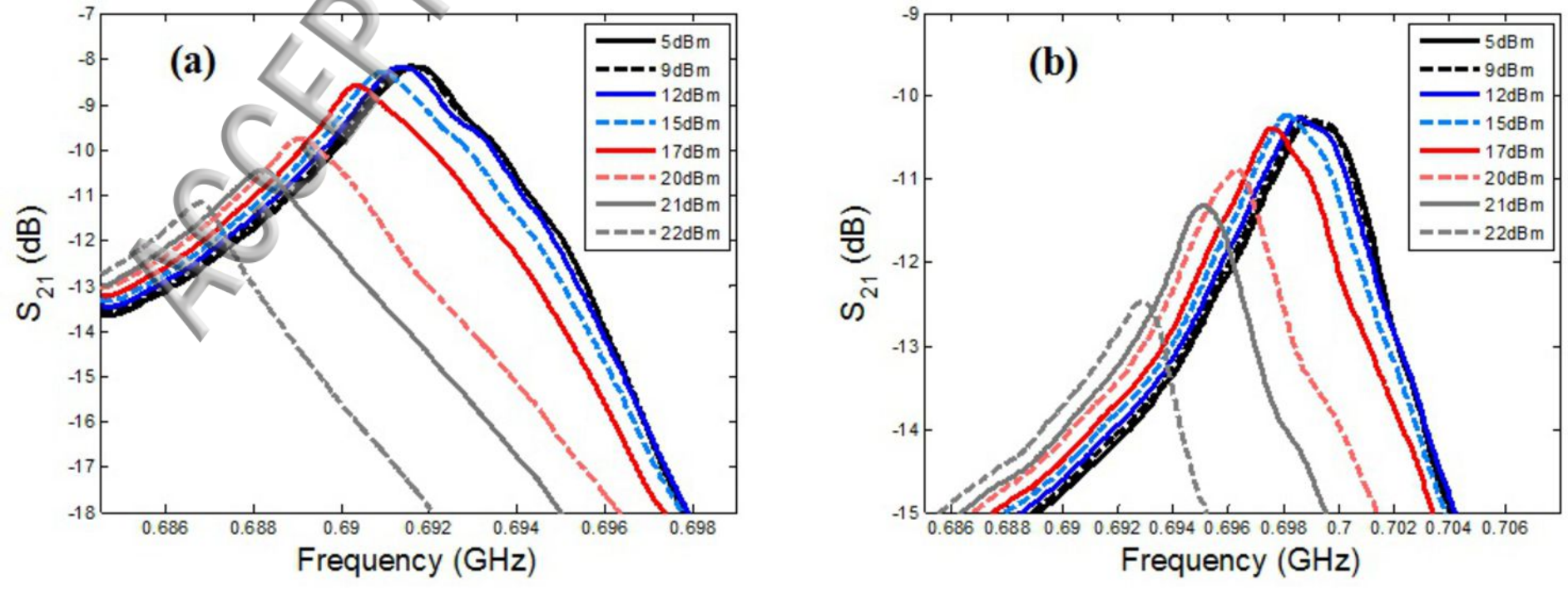
(a)
(b)
5dBm
9dBm
12dBm
15dBm
17dBm
20dBm
21dBm
22dBm
S21 (dB)
Frequency (GHz)
-7
-8
-9
-10
-11
-12
-13
-14
-15
-16
-17
-18
0.686
0.688
0.69
0.692
0.694
0.696
0.698
0.7
0.702
0.704
0.706

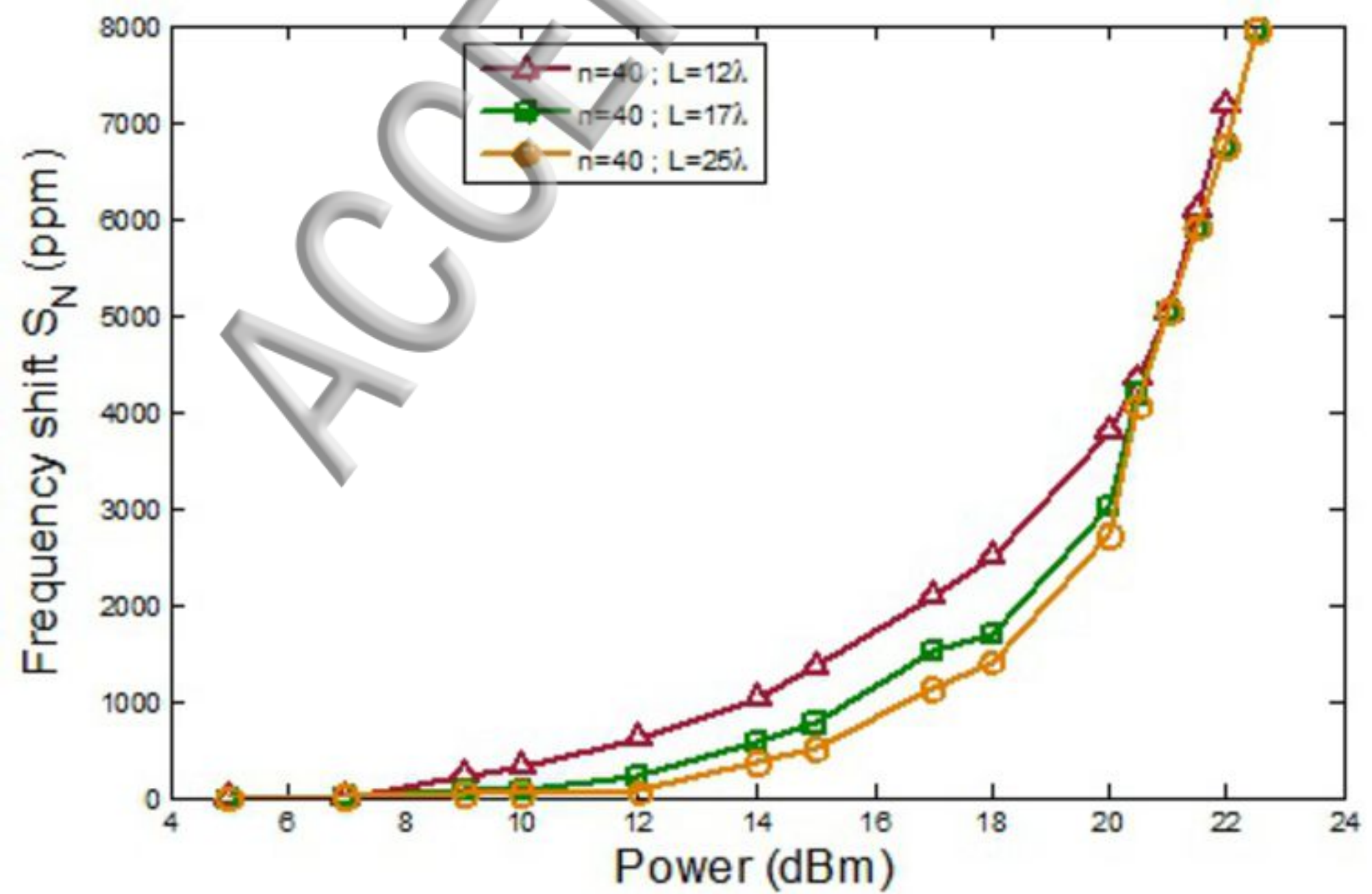
n=40 ; L=12λ
n=40 ; L=17λ
n=40 ; L=25λ
Frequency shift S_N (ppm)
Power (dBm)
0
1000
2000
3000
4000
5000
6000
7000
8000
4
6
8
10
12
14
16
18
20
22
24

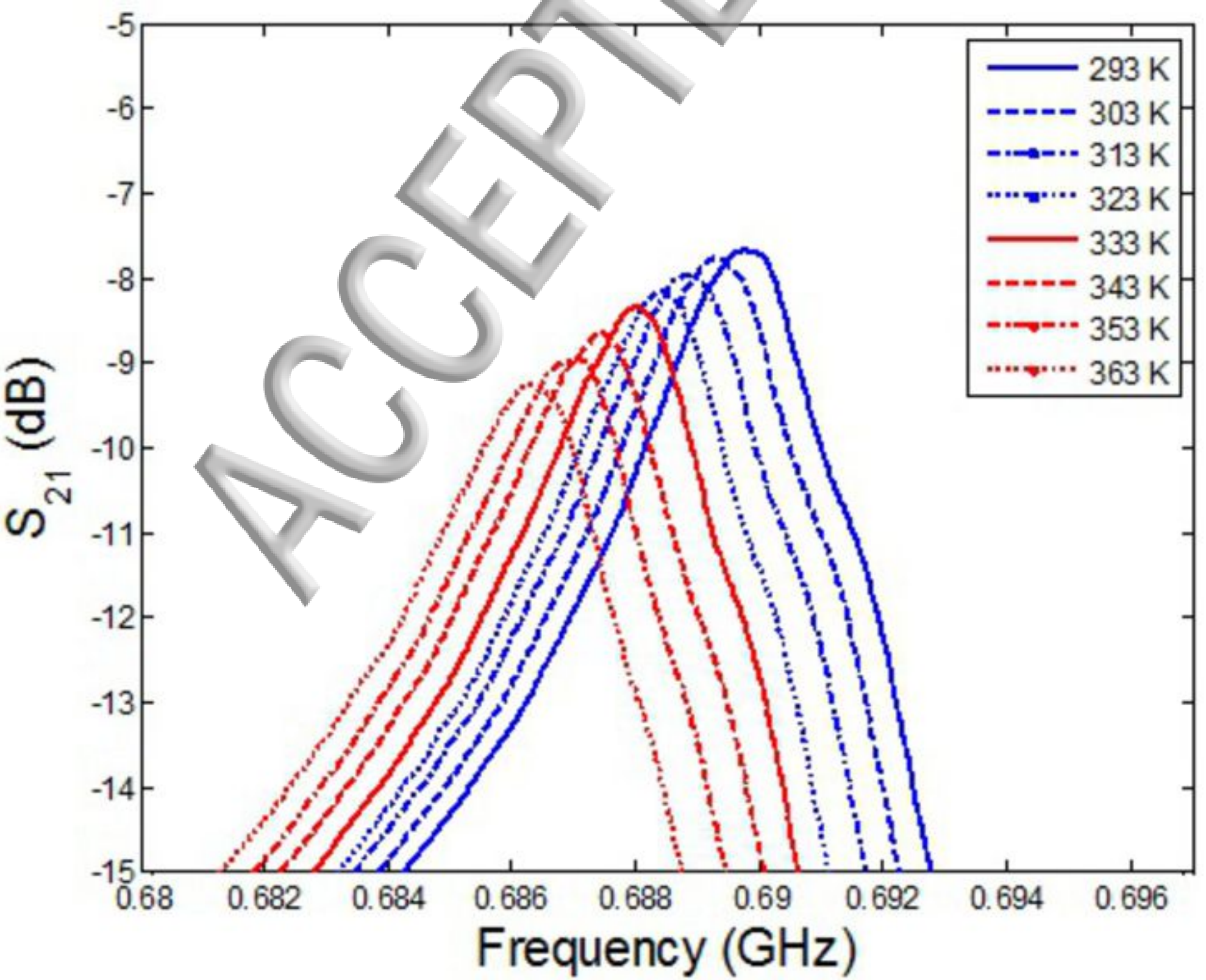
293 K
303 K
313 K
323 K
333 K
343 K
353 K
363 K
S21 (dB)
-5
-6
-7
-8
-9
-10
-11
-12
-13
-14
-15
0.68
0.682
0.684
0.686
0.688
0.69
0.692
0.694
0.696
Frequency (GHz)

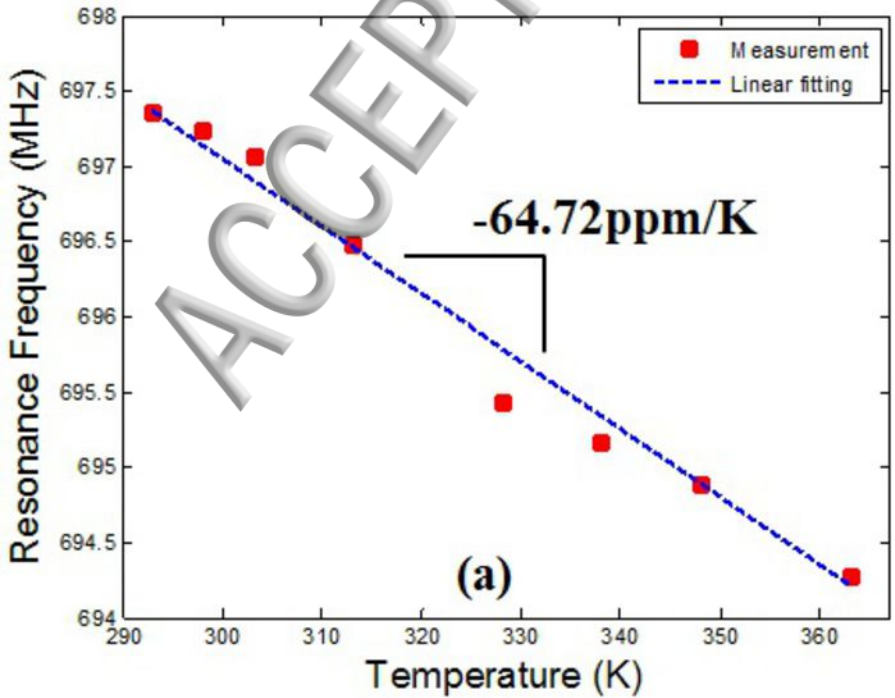
Measurement
Linear fitting
-64.72ppm/K
(a)
Resonance Frequency (MHz)
Temperature (K)
698
697.5
697
696.5
696
695.5
695
694.5
694
290
300
310
320
330
340
350
360

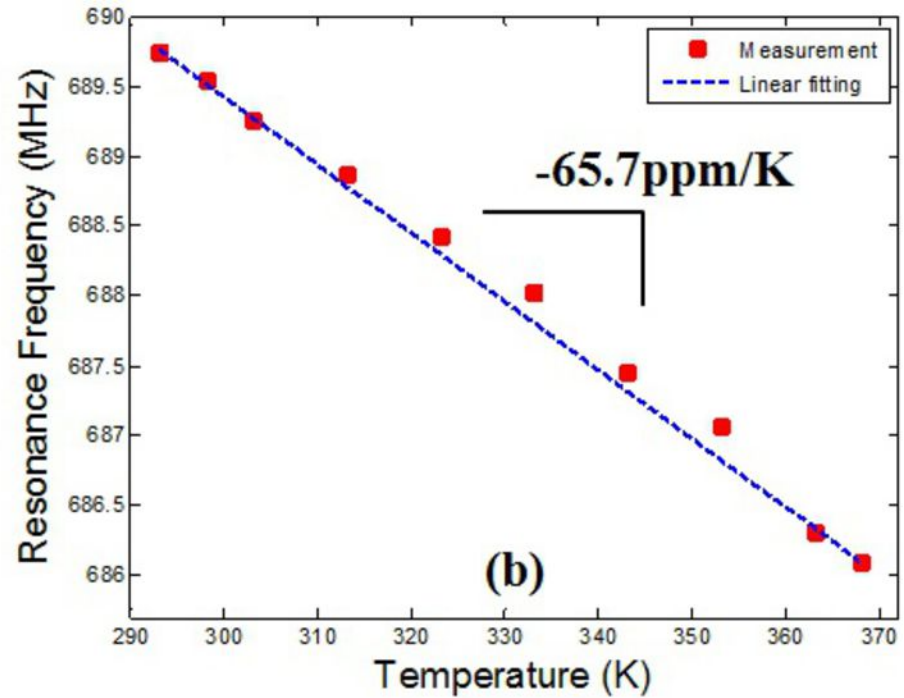
Measurement
Linear fitting
-65.7ppm/K
(b)
Resonance Frequency (MHz)
Temperature (K)
690
689.5
689
688.5
688
687.5
687
686.5
686
290
300
310
320
330
340
350
360
370